https://doi.org/10.5194/egusphere-2025-6030
Preprint. Discussion started: 20 January 2026

Seasonal and interannual variability of precipitation and rainfall erosivity in Northeastern Japan: insights from 14 years of observations after Fukushima Dai-ichi nuclear accident (2011-2024)

Thomas Chalaux-Clergue[1,2], Pierre-Alexis Chaboche[1], Yoshifumi Wakiyama[3,4], and Olivier Evrard[1,4]

[1]Laboratoire des Sciences du Climat et de l'Environnement (LSCE, IPSL), Université Paris-Saclay, UMR 8212 (CEA, CNRS, UVSQ), Gif-sur-Yvette, 91190, France
[2]Water and Soil Resources Research, Institute of Geography, Universität Augsburg, Augsburg, 86150, Germany
[3]Institute of Environmental Radioactivity (IER), University of Fukushima, Fukushima, 960-1296, Japan
[4]MITATE Lab, International Research Laboratory - IRL 2039 (CNRS, CEA, Fukushima University, Fukushima, 960-1296, Japan

Correspondence: Thomas Chalaux-Clergue (thomaschalaux@icloud.com) and Olivier Evrard (oliver.evrard@lsce.ipsl.fr)

Abstract. The Fukushima Dai-ichi Nuclear Power Plant (FDNPP) accident in March 2011, led to the deposition of about 2.0 PBq of ^{137}Cs across Fukushima Prefecture, resulting in widespread long-term environmental contamination. The accumulation of ^{137}Cs in the uppermost soil layer, led rainfall-driven soil erosion to become a major mechanism for ^{137}Cs redistribution across the landscape. Previous research (Laceby et al., 2016a), which analysed data over 1995-2015, identified the June-October period as critical for rainfall erosivity. However, this analysis covered only the immediate five years period after the accident, leaving spatial and temporal patterns, event-scale dynamics, and long-term trends unquantified in the longer post-accidental context. To address this gap, the current research analysed 10-minute precipitation records from 58 weather stations located within a 110-km radius of the FDNPP, to include most of ^{137}Cs deposition onland, during the 14 years that followed the accident (2011–2024), calculating event-level precipitation amount and rainfall erosivity (EI_{30}), and aggregating metrics across annual, monthly, seasonal, and extreme-event timescales. Between 2011 and 2024, median annual precipitation was 1318 mm, with erosive events contributing 917 mm and generating 3,290 $\mathrm{MJ\,mm\,ha^{-1}\,h^{-1}}$ of erosivity. The June-October period accounted for 61 % of erosive events, representing 46 % of annual precipitation (602 mm) but 86 % of annual erosivity (2,698 $\mathrm{MJ\,mm\,ha^{-1}\,h^{-1}}$), with a clear precipitation-erosivity relation (r^2 = 0.62). Erosivity was highly concentrated during a few extreme events: the three most erosive events of each year contributed 55 % of total annual erosivity (1,753 $\mathrm{MJ\,mm\,ha^{-1}\,h^{-1}}$; 224 mm), whilst the single most erosive event alone accounted for 28 % (912 $\mathrm{MJ\,mm\,ha^{-1}\,h^{-1}}$; 94 mm). In 2011, 2015, and 2019, single events dominated annual erosivity, generated 38-44 % of annual erosivity. These findings quantify the erosive drivers of ^{137}Cs remobilisation since the accident with at large spatial and a high temporal resolution, supporting the retrospective reconstruction and prediction of long-term contamination dynamics. The predominance of extreme rainfall events emphasises their role in controlling sediment and contaminant transport in the post-accidental Fukushima context. All datasets, reproducible analytical workflows, and scripts (R package RainErosivity) are openly available via Zenodo and GitHub, supporting research on rainfall-driven ^{137}Cs redistribution, sediment transfer, erosion risk assessment and long-term geomorphological evolution of catchments.

https://doi.org/10.5194/egusphere-2025-6030
Preprint. Discussion started: 20 January 2026

1 Introduction

In March 2011, the Fukushima Dai-ichi Nuclear Power Plant (FDNPP) accident led to the release of a considerable amount of radionuclides, of which about 20 % were deposited over Japan (Morino et al., 2013; Onda et al., 2020). Among these, ^{137}Cs remains of particular concern because of its relatively long half-life (30 years) and its potential impacts over the long term on the environment and human health. The total inland deposition of ^{137}Cs was estimated to 2.7 PBq, of which, 74 % were deposited within the Fukushima Prefecture (Kato et al., 2019; Taniguchi et al., 2019). It is estimated that about 83 % of the Prefecture area (11,430 km^2) received more than 5 $\mathrm{kBq\,m}^{-2}$ of ^{137}Cs, with 26 % being exposed to more than 100 $\mathrm{kBq\,m}^{-2}$ (Kato et al., 2019).

After deposition, ^{137}Cs is rapidly and quasi-permanently adsorbed to fine soil particles (silt and clay; Saito et al., 2014; Nakao et al., 2014, 2015). Consequently, 90-99 % of the radiocesium inventory has accumulated in the upper 5 cm of undisturbed soils (Kato et al., 2012; Lepage et al., 2015; Konoplev et al., 2016). This strong binding has limited the transfer of ^{137}Cs from soil to plants, both in annual or perennial herbaceous and tree species (Yamashita et al., 2014; Tamaoki et al., 2016; Onda et al., 2020). As a result, deposited ^{137}Cs remained mainly concentrated in the upper organo-mineral soil layer, rendering it particularly vulnerable and susceptible to downstream transfers following water erosion during rainfall events (Wakiyama et al., 2019; Ikenoue et al., 2020).

During the last 14 years, river system in the eastern part of Fukushima Prefecture have demonstrated a high reactivity to intense rainfall events (Chartin et al., 2013; Evrard et al., 2014, 2020). In the steep and mountainous catchments of this region, such intense events were associated with substantial soil erosion and sediment export, thereby contribute to the downstream transfer of contaminated material to the Pacific Ocean (Evrard et al., 2014; Uchiyama et al., 2022; Diacre et al., 2023). The transfer of ^{137}Cs in the river system occurs predominantly in particulate form (96.5 %; Taniguchi et al., 2019) associated to suspended sediment matter (Sakaguchi et al., 2015; Evrard et al., 2015). However, it has been determined that a limited number of these high-intensity rainfall events were responsible for the majority of particulate ^{137}Cs fluxes (Sakaguchi et al., 2015; Kitamura et al., 2016; Konoplev et al., 2018), accounting for 82–99 % of total annual transfers (Yamashiki et al., 2014; Iwagami et al., 2017; Osawa et al., 2018).

The magnitude of radiocesium transport depends on several factors influencing soil erosion, including rainfall erosivity, topography, land use, and soil properties (Yoshimura et al., 2015; Wakiyama et al., 2019). To reflect the relationship between precipitation (raindrop splash and runoff scour) and soil loss, Wischmeier and Smith (1958) developed the EI_{30} index. The annual R-factor was subsequently defined as the summation of these event-based EI_{30} values over a year (Wischmeier and Smith, 1958). This factor was later incorporated into the USLE and its subsequent revisions, RUSLE (Renard et al., 1997) and RUSLE2 (USDA–ARS, 2013). Conventionally, the R-factor is estimated as a long-term average annual erosivity, typically about 20 to 30 years (Renard and Freimund, 1994; Wischmeier and Smith, 1978), a practice designed to smooth out interannual variability.

https://doi.org/10.5194/egusphere-2025-6030
Preprint. Discussion started: 20 January 2026

However, in the Fukushima region, heavy precipitation events, such as tropical storms, typhoons, or linear precipitation bands, have been highlighted as a key driver of radiocesium transfer at the catchment scale, exhibiting strong intra-annual variability associated with seasonal climatic patterns (Laceby et al., 2016a; Vandromme et al., 2023). Over the 1995–2015 period, Laceby et al. (2016a) reported that the majority of annual precipitation (60 %) and rainfall erosivity (86 %) occurred between June and October, with tropical cyclones alone accounting for about 22 % of precipitation and 40 % of erosivity. Given this context, in the present study, EI_{30} values and annual and seasonal R-factors were utilised to compare the relative intensity of individual events or their cumulative impact over specific periods (e.g., annually, seasonally). This approach allows for the contextualisation of their occurrence, seasonality, and evolution since 2011, thereby assessing the potential for erosion and subsequent radiocesium transfer. Nonetheless, other parameters, such as seasonal variations in vegetation cover and antecedent soil moisture, also modulate soil erosion capacity (Yoshimura et al., 2015; Vandromme et al., 2023). Erosive events occurring during full canopy conditions generally produce less erosion than those that occurs early in spring or late in autumn.

Therefore, this study provides an updated characterisation of precipitation and rainfall erosivity from 2011 to 2024 within a 110 km radius region around FDNPP, comprising most catchments draining the main radioactive plume contaminated with ^{137}Cs. Based on high-resolution (10-min) rainfall records compiled from 58 weather stations, it aims to (i) quantify the inter- and intra-annual variability of precipitation and rainfall erosivity, (ii) determine the most relevant temporal scale for regional and interannual comparisons, and (iii) assess the contribution of the most erosive rainfall events to seasonal and annual cumulative precipitation and rainfall erosivity. The resulting precipitation and rainfall erosivity metrics, computed at annual, monthly and seasonal scales, as well as for the most erosive events, are provided for the Fukushima region from 2011 to 2024. These metrics can then be used to conduct future research regarding rainfall erosivity and its implications for long-term management of sediment and radiocesium transfers in the region.

2 Materials and Methods

2.1 Study area

Of all the radiocesium released during the FDNPP accident, most of the ^{137}Cs deposited on terrestrial environments (2.7 PBq) accumulated within Fukushima Prefecture (2.0 PBq) (Kato et al., 2019; Taniguchi et al., 2019). The area investigated in this study, located within a 110-km radius around the FDNPP (17,000 km^2), received most of this initial fallout (Fig. 1).

Most of the deposition occurred in two main geographical regions of Fukushima Prefecture: the Hama-dori and Naka-dori regions, which are separated by the north-south-trending Abukuma mountain range (Nakao et al., 2014). The western boundary of the Naka-dori region is bordered by the Ōu mountain range. Hydrologically, the two regions differ. The Naka-dori region largely corresponds to the Abukuma River Basin (5,200 km^2), whereas the Hama-dori region is drained by several small coastal catchments (covering typically surface areas $\leq$ 700 km^2). These coastal catchments may generally be subdivided into two parts: a steep, mountainous upper section within the Abukuma mountain range, which transitions abruptly into a flat coastal plain. According to Köppen's climatic classification, from East to West, the coastal plains of the Hama-dori region are exposed

https://doi.org/10.5194/egusphere-2025-6030
Preprint. Discussion started: 20 January 2026

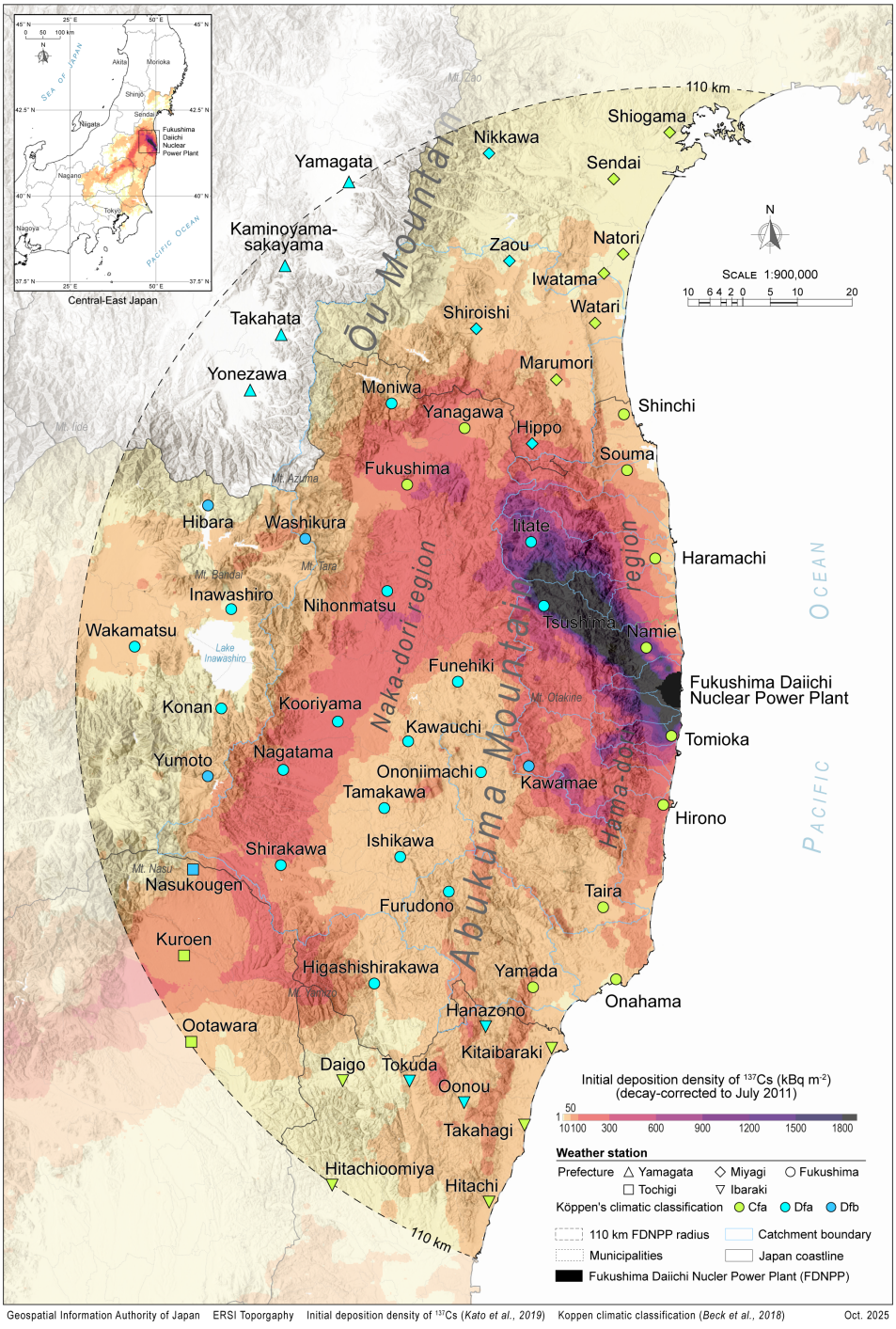

Figure 1. Location of the 58 weather stations within a 110-km radius around the Fukushima Dai-ichi Nuclear Power Plant (FDNPP) over the ^{137}Cs deposition on soils across Northeastern Japan after Kato et al. (2019). Cartographic data available from the Geospatial Information Authority of Japan - GSI).

https://doi.org/10.5194/egusphere-2025-6030
Preprint. Discussion started: 20 January 2026

to a Cfa temperate climate with no dry season and hot summer, which shifts to a Dfa cold climate with no dry season and hot summer when reaching the foothills of the Abukuma mountain range within the mountainous part of the Hama-dori region and the whole Naka-dori region (Beck et al., 2018). With increasing elevation, some areas of the Abukuma mountains transition from hot (Dfa) to warm summer (Dfb) (e.g. Kawamae or Hibara stations).

The regional precipitation regime is driven by tropical cyclones, with a few extreme events accounting for a large proportion of the annual rainfall volume and intensity (Chartin et al., 2013; Evrard et al., 2014). The period from May to October, corresponding to the Japanese typhoon season, contributes to about 60 % of the annual precipitation and 86 % of the rainfall erosivity, with a peak from July to September (Laceby et al., 2016a). Over the last 30-years period (1991-2021), the mean annual temperature in the Fukushima region was 13.4 $\pm$ 0.5 $^{\circ}\mathrm{C\,y^{-1}}$ (standard deviation = SD), ranging on average from -1.5 $\pm$ 0.9 $^{\circ}\mathrm{C}$ to 30.5 $\pm$ 2.1 $^{\circ}\mathrm{C}$ in January and August, respectively. The mean annual precipitation was to 1207 $\pm$ 216 $\mathrm{mm\ y^{-1}}$ (SD) (Chalaux-Clergue et al., 2024a).

2.2 Weather stations

Precipitation and temperature records every 10 $\mathrm{minutes}$ from 1 January 2011 to 31 December 2024 were downloaded from 58 automated weather stations, available from the Automated Meteorological Data Acquisition System stations (AMeDAS) operated by the Japanese Meteorological Agency (JMA) or stations operated by Prefectural Authorities, within a 110 km radius around the FDNPP (JMA, 2024, in Japanese) (Fig. 1). Previous research has shown the reliability of the 10 min rainfall dataset from JMA, indicating that further correction was not required (Shiono et al., 2013; Duan et al., 2015; Laceby et al., 2016a; Chartin et al., 2017).

2.3 Precipitation and rainfall erosivity

Erosive events were identified and extracted from the data according to two criteria: (1) individual events were required to accumulate precipitation greater than 12.7 mm (Wischmeier and Smith, 1978; Panagos et al., 2015) and (2) cumulative precipitation of less than 1.27 mm over a period of 6 h was required to discretize events (Wischmeier and Smith, 1978; Renard and Freimund, 1994; Yin et al., 2017). To account for the potential occurrence of snowfall, precipitation records were removed when the temperature was below 0 $^{\circ}\mathrm{C}$, when available (Meusburger et al., 2012).

The event rainfall erosivity, EI_{30} in $\mathrm{MJ\,mm\,ha^{-1}\,h^{-1}}$, was calculated for each erosive event that occurred over the study period for each weather station. It was calculated as the product of the energy of the precipitation event (E, in $\mathrm{MJ\,ha^{-1}}$) and its maximum 30-$\mathrm{minutes}$ intensity (I_{30}, in $\mathrm{mm\,h^{-1}}$) (Brown and Foster, 1987; Renard and Freimund, 1994; Yin et al., 2017):

$$EI_{30} = \left(\sum_{r=1}^{l} e_r \, v_r \right) I_{30} \tag{1}$$

where e_r represents the surface precipitation energy per unit of precipitation ($\mathrm{MJ\ ha^{-1}\ mm^{-1}}$), and v_r is the volume of precipitation (mm) during a given time interval (i.e., 10-min in the current research) for the r^{th} time interval of the event from

https://doi.org/10.5194/egusphere-2025-6030
Preprint. Discussion started: 20 January 2026

1, the first precipitation record during the event, to l, the last record of the event. For each time interval, e_t was calculated using the RUSLE2 corrected formula of Brown and Foster (1987) Yin et al. (2017) (0.082 vs. 0.05):

$$e_r = 0.29\left(1 - 0.72\, e^{-0.082\, i_r}\right) \tag{2}$$

where i_r is the precipitation intensity ($\mathrm{mm\,h^{-1}}$, i.e., $6 \times v_i$).

For each period (year, month or season), the R-factor was then calculated as the sum of the EI_{30}s of events that occurred over a defined period (i.e., year, month, or season):

$$R = \sum_{i=1}^{n} EI_{30\ i} \tag{3}$$

where i is the i^{th} erosive event out on n events that occurred during the period.

The identification of erosive events and calculation of event rainfall erosivity and event cumulative precipitation were performed in R language using the RainErosivity package (Chalaux-Clergue, 2025, version 1.1.0).

2.4 Calculation of metrics

All statistical analyses were performed at the station level before being aggregated to broader spatial and temporal scales. For each monitoring station, annual, monthly, and seasonal (June-October) precipitation and rainfall erosivity totals, were first calculated individually according to the temporal resolution. These station-level values were then used to derive annual, monthly or seasonal regional metrics by computing the corresponding median, 25th and 75th quantiles (interquartile range - IQR), mean and standard deviation (SD) across all stations operating during the temporal resolution under consideration. In addition, long-term pluriannual metrics were obtained by aggregating all station-level data over the entire study period and calculating the same summary metrics. This hierarchical approach allowed preserving the local variability while ensuring a consistent comparison of temporal and spatial patterns. The use of medians was intended to highlight persistent differences between the different temporal resolutions and to reduce the influence of extreme events, thereby improving the interpretation of seasonal patterns and typical behaviours.

To check for temporal and spatial consistence across the years, months or seasons and to assess which of those display statistically similar behaviours at the station-level, non-parametric Sign pairwise tests were performed on station-level values. The sign test assesses the occurrence of consistent differences between pairs of observations, without any assumption on the nature of their distribution.

The sign test compares the station pairs values, assigning a positive or negative sign depending on whether one station's value exceeded the other or not. The number of positive differences was reported as the number of successes out of the number of station pairs to perform a two-sided exact binomial test (eq. Bernouilli experiment) with a confidence level of 0.5 (performed

https://doi.org/10.5194/egusphere-2025-6030
Preprint. Discussion started: 20 January 2026

with the binom.test function from stats package). A Bonferroni correction, corresponding to the number of comparisons realised (i.e., 91 for 14 years; 66 for 12 months), was applied on the p values resulting from the binomial test. Then, pairs with a p value greater than $\alpha = 0.5$ were considered to be non-statistically different. Based on these results, non-statistically different years were grouped accordingly. It was ensured that for each pair comparison only operating stations were considered.

This approach allowed to identify non-statistically distinguishable years, months or seasons at the station level, which allowed to identify zones/stations sharing temporal and spatial consistency among the region.

All processing, analyses and modelling were performed using the R programming environment (R Core Team, 2025, version 4.5.1) in RStudio (Posit team, 2025, version 2025.09.1+401).

3 Results

3.1 Annual and Monthly variability

3.1.1 Precipitation

Annual precipitation across the 58 weather stations within a 110 km radius around FDNPP exhibited moderate interannual variability over the 2011-2024 period (Fig. 2.A.c). The median annual cumulative precipitation ranged from 1,119 [1,012-1,293] $\mathrm{mm\,yr^{-1}}$ (IQR) in 2018 to 1581 [1382-1763] $\mathrm{mm\,yr^{-1}}$ in 2014, with a pluriannual median of 1,318 [1,148-1,501] $\mathrm{mm\,yr^{-1}}$ and a mean of 1,360 $\pm$ 301 $\mathrm{mm\,yr^{-1}}$ (SD) (Appendix Table A1). The low difference (3 %) between pluriannual median and mean values supports this moderate interannual variability.

Among the fourteen years under consideration, nine to ten years (64-71 %) were within the same sign-test statistical groups (i.e., groups b, f, and i), indicating similar values and spatial distributions at the station level (Fig. 2.A.c). Nonetheless, two narrower groupings, c-e and d-h, respectively included the years with the highest (2014, 2019, 2020, 2021) and lowest cumulative precipitation (2018, 2022, 2023, 2024), highlighting differences, although moderate, in precipitation regimes.

At the station level, annual precipitation showed a spatial gradient across the study area (Fig. 3.a; Appendix Table A1). The highest annual cumulative precipitation was often recorded at Washikura (Fukushima Pref., central-eastern part of the study area), Nasukougen (Tochigi Pref., south-eastern part) and Hanazono (Ibaraki Pref., southern part). In contrast, the lowest values were consistently recorded at Yanagawa (Fukushima Pref., central-northern part), Inawashiro (Fukushima Pref., central-eastern part), and Kaminoyamasakayama (Yamagata Pref., north-eastern part). The constancy of these spatial contrasts and patterns throughout most years, indicated the occurrence of stable regional precipitation patterns at the annual scale.

At the monthly scale, cumulative precipitation exhibited a pronounced seasonal pattern (Fig. 2.A.a and b). The driest months were February and January, closely followed by December and November, while the wettest months were September and July.

https://doi.org/10.5194/egusphere-2025-6030
Preprint. Discussion started: 20 January 2026

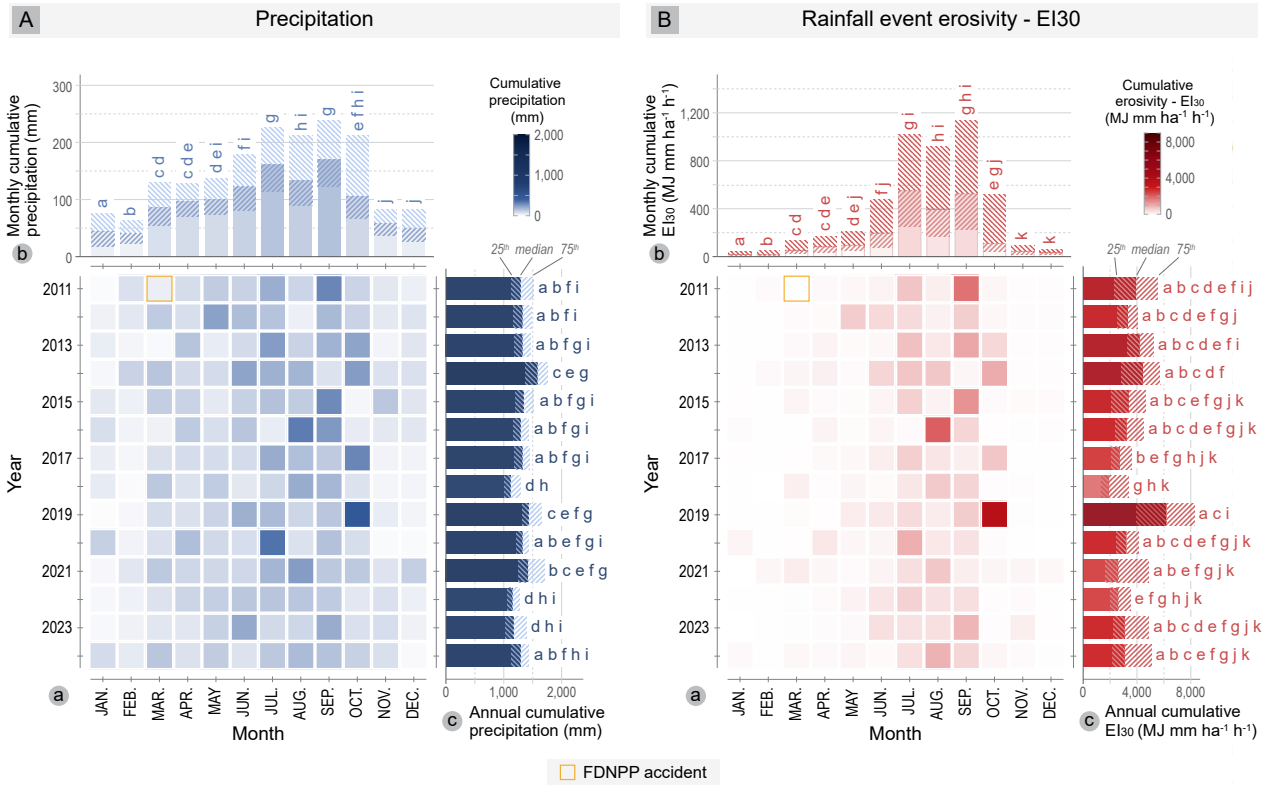

Figure 2. Inter-annual variability of (a) cumulative monthly median of [A] precipitation and [B] rainfall erosivity (2011-2024), together with (b) monthly and (c) annual distributions (median, 25th and 75th percentiles), with station-level paired Sign test groupings (p value ≥ 0.05) from 58 weather stations located within a 110 km radius around FDNPP.

Median monthly totals ranged from 39 [23-64] $\mathrm{mm\,mo^{-1}}$ in January to 170 [123-238] $\mathrm{mm\,mo^{-1}}$ in September and 162 [114-227] $\mathrm{mm\,mo^{-1}}$ in July (Appendix Table A2). Sign tests groupings statistically distinguish between the group of months from June to October, forming a high-precipitation period that was clearly separated from the low-precipitation months from November to February (Fig. 2.A.b). Within this high-precipitation period, a further subdivision was made between July and September (group g), corresponding to the wettest months, and June, August, and October (groups f, h, i).

Monthly IQR were also higher during the June to October period, increasing from 98 $\mathrm{mm\,mo^{-1}}$ in June to 146 $\mathrm{mm\,mo^{-1}}$ in October, highlighting some interannual variability. In addition, the highest total monthly precipitation recorded between June and October showed a clear spatial pattern (Appendix Fig. 4.a and Table A2). The highest values for the period from June to August were recorded at Washikura (Fukushima Pref., central-eastern part), with 575 $\mathrm{mm\,mo^{-1}}$ in June 2014, 622 $\mathrm{mm\,mo^{-1}}$ in July 2020, and 932 $\mathrm{mm\,mo^{-1}}$ in August 2016. Similarly, the highest monthly cumulative precipitation for September and October was recorded at Hippo (Miyagi Pref., central part), with 673 $\mathrm{mm\,mo^{-1}}$ in 2015 and 902 $\mathrm{mm\,mo^{-1}}$ in 2019. More exceptionally, high precipitation was recorded in May 2012 at Oonou (Ibaraki Pref., central-southern part) with 536 $\mathrm{mm\,mo^{-1}}$. Conversely, local monthly minima showed limited temporal recurrence across stations.

https://doi.org/10.5194/egusphere-2025-6030
Preprint. Discussion started: 20 January 2026

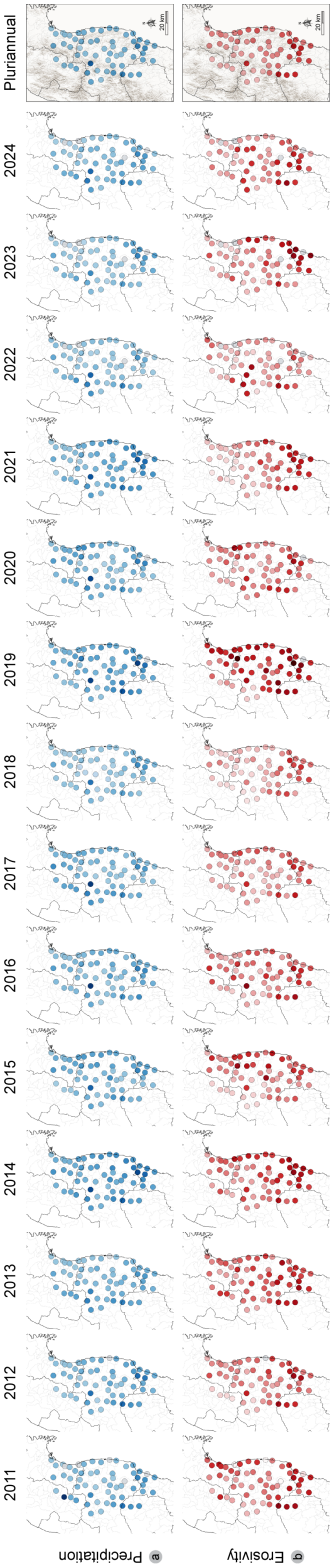

Figure 3. Annual records and pluriannual median values of annual cumulative (a) precipitation and (b) rainfall erosivity over the period 2011-2024 across the 58 weather stations located within a 110-km radius around FDNPP.

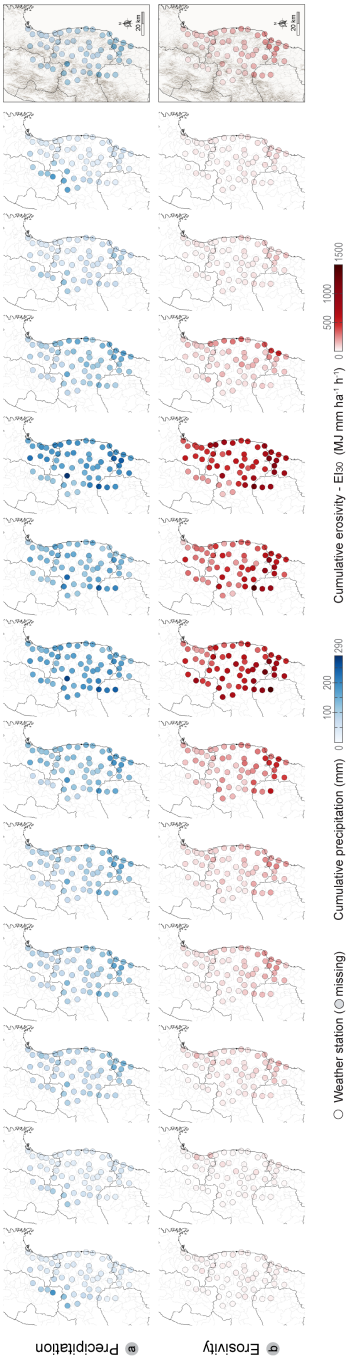

Figure 4. Monthly records and plurimonthly median values of cumulative (a) precipitation and (b) rainfall erosivity over the period 2011-2024 across the 58 weather stations located within a 110-km radius region around FDNPP.

https://doi.org/10.5194/egusphere-2025-6030
Preprint. Discussion started: 20 January 2026

3.1.2 Rainfall erosivity

Between 2011 and 2024, a median of 37 [23-31] (IQR) erosive events occurred annually across the region, generating a median annual rainfall erosivity (EI_{30} or *R*-factor) ranging from 1,908 [1,388-3,392] $\mathrm{MJ\,mm\,ha^{-1}\,h^{-1}\,yr^{-1}}$ in 2018 to 6,159 [3,970-8,270] $\mathrm{MJ\,mm\,ha^{-1}\,h^{-1}\,yr^{-1}}$ in 2019 (Fig. 2.B.c). The pluriannual median of 3,290 [2,273-4,947] $\mathrm{MJ\,mm\,ha^{-1}\,h^{-1}\,yr^{-1}}$ and the mean of 3,868 $\pm$ 2,327 $\mathrm{MJ\,mm\,ha^{-1}\,h^{-1}\,yr^{-1}}$ differed by 15 % which, along with high IQR (2674 $\mathrm{MJ\,mm\,ha^{-1}\,h^{-1}\,yr^{-1}}$) and SD, indicated a high interannual variability (Appendix Table A3).

Despite this high variability, ten to twelve (71-86 %) years among those investigated remained within the same sign-test statistical groups (i.e., groups a, b, c, e, f, g, and j), indicating high similarities at the station level (Fig. 2.B.c). Nonetheless, two narrower groupings, h and i, respectively included the years with the highest (2011, 2013, 2019 in i) and lowest total cumulative precipitation (2017, 2018, 2022 in h), highlighting that these two extreme regimes may be differentiated at the station level.

At the station level, the highest annual cumulative rainfall erosivity was the most frequently recorded in the southern part of the study area (i.e., Daigo, Hanazono, Hitachi, Kuroen, Nasukougen, Ootawara, and Yamada), and least frequently in the central-western (e.g., Kawauchi, Nihonmatsu, Washikura) or central-northern regions (e.g., Shinchi) (Fig. 3.a; Appendix Table A3). During most years, the local maxima commonly amounted to around 10,000 $\mathrm{MJ\,mm\,ha^{-1}\,h^{-1}\,yr^{-1}}$ (2011, 2012, 2013, 2014, 2015, 2016, 2023, and 2024), or between 6,000 and 9,000 $\mathrm{MJ\,mm\,ha^{-1}\,h^{-1}\,yr^{-1}}$ (2017, 2018, 2020, 2021, and 2022). Clearly, 2019 provided an exception, as the Hanazono station recorded a value of 18,004 $\mathrm{MJ\,mm\,ha^{-1}\,h^{-1}\,yr^{-1}}$, which was 5.5 times higher than the pluriannual median.

At the monthly scale, rainfall erosivity exhibited a very pronounced seasonal pattern (Fig. 2.B.b). The least erosive months were February, November, January, and December, while the most erosive months were September and July. Median total monthly values ranged from 32 [19-48] $\mathrm{MJ\,mm\,ha^{-1}\,h^{-1}\,mo^{-1}}$ in February to 124 [77-182] $\mathrm{MJ\,mm\,ha^{-1}\,h^{-1}\,mo^{-1}}$ in July and 140 [88-207] $\mathrm{MJ\,mm\,ha^{-1}\,h^{-1}\,mo^{-1}}$ in September (Appendix Table A4). This strong seasonality was also reflected in the frequency of erosive events, with a median of one event per month from November to February; two events from March to May, and even three to four events per month during the June-October period. Sign tests also confirmed the strong seasonality by statistically distinguishing low- and high-erosivity months. The low-erosivity period, from November to March, was divided into three groups (groups a, b, k) despite similar median values (19-44 $\mathrm{MJ\,mm\,ha^{-1}\,h^{-1}\,yr^{-1}}$). The high-erosivity period, from June to October, revealed finer distinctions: July and September provided the most erosive group (g), showing some overlap with August (groups h and i), while June and October were grouped together (f and j) and showed some similarity with May (e). Spring months, from March to May, were globally grouped together (c, d, e), marking a transitional phase between the two main erosive seasons.

Monthly IQR were also the highest during June to October period, increasing from 98 $\mathrm{MJ\,mm\,ha^{-1}\,h^{-1}\,mo^{-1}}$ in June to 155 $\mathrm{MJ\,mm\,ha^{-1}\,h^{-1}\,mo^{-1}}$ in October, highlighting the occurrence of some interannual variability. In July and September, IQRs represented about 0.8-0.9 times their respective medians, whereas for June, August, and September, this ratio ranged

https://doi.org/10.5194/egusphere-2025-6030
Preprint. Discussion started: 20 January 2026

from 1.1 to 1.9, further indicating the occurrence of pronounced interannual variability among these months (Fig. 2.B.c and Appendix Table A4)).

During high-erosivity months, the highest monthly records were generally observed in the southern part of the study area (Hanazono in June 2012, Shirakawa in July 2019, and Hitachi in September 2023) or in the central part (Washikura in August 2016 and Hippo in October 2019) (Fig. 3.a, Appendix Table A2). In July and August, local maxima reached around 10,000 $\mathrm{MJ\,mm\,ha^{-1}\,h^{-1}\,mo^{-1}}$ in 2016 at Washikura and in 2023 at Hitachi, respectively, and nearly 15,000 $\mathrm{MJ\,mm\,ha^{-1}\,h^{-1}\,mo^{-1}}$ in October 2019 at the Hippo station. Outside of this period, high monthly erosivity total values were also recorded during spring months. This was observed for instance at Taira station (Fukushima Pref., southern part) with 5,402 $\mathrm{MJ\,mm\,ha^{-1}\,h^{-1}\,mo^{-1}}$ in April 2013, and at Ootawara (Tochigi Pref., south-east part) with 3,582 $\mathrm{MJ\,mm\,ha^{-1}\,h^{-1}\,mo^{-1}}$ in May 2012. Conversely, local monthly minima showed limited temporal or spatial recurrence across stations.

3.2 Typhoon season dynamics (June-October)

3.2.1 Seasonal contribution and interannual variability

During the five-month period from June to October, the median number of erosive events ranged from 13-15 events in 2011, 2012, 2015, 2018 and 2022, to 17-19 events in 2013, 2014, 2016, 2017, 2019, 2020 and 2021, with a pluriannual median of 16 [14-19] events (IQR), representing about 61 % of the median annual number of events (Fig. 5).

Seasonal rainfall erosivity (from June to October) represented a pluriannual median of 2,698 [1,826-4,076] $\mathrm{MJ\,mm\,ha^{-1}\,h^{-1}}$ and a mean of 236 $\pm$ 2,121 $\mathrm{MJ\,mm\,ha^{-1}\,h^{-1}}$, accounting for 86 and 83 % of total annual cumulative (Fig. 5.B.a). Seasonal median cumulative values ranged from 1,560 [1,016-2,756] $\mathrm{MJ\,mm\,ha^{-1}\,h^{-1}}$ in 2018 to 5,681 [3,765-7,377] $\mathrm{MJ\,mm\,ha^{-1}\,h^{-1}}$ in 2019, along with relative contribution to the total annual values ranging from 70 % in 2021 to 93 % in 2019. The difference between the pluriannual median and mean was about 17 %. Together with the wide IQR (2,250 $\mathrm{MJ\,mm\,ha^{-1}\,h^{-1}}$) and standard deviation, this finding highlights the strong interannual variability in seasonal erosivity (Appendix Table A5). Nonetheless, across the period, the relative contribution of the season to annual values ranged from 70 % in 2021 to 93 % in 2019.

Despite this high variability, nine to eleven years were found within the same sign test statistical groups (i.e., groups a, b, e, f, g, and j), indicating overall spatial consistency in seasonal erosivity patterns (Fig. 5.B.a, 6.c). Three narrower groupings: h, c, and d (with c and d differing only by the inclusion of 2015 in group c), respectively regrouped years with lower (2012, 2018, 2021, 2022) and higher seasonal totals (2011, 2013, 2014, 2015, 2016, 2023). Lower-erosivity years (group h) exhibited total seasonal values around 2,000-2,308 $\mathrm{MJ\,mm\,ha^{-1}\,h^{-1}}$, whereas higher-erosivity years ranged from 2,675 [1,817-4,352] $\mathrm{MJ\,mm\,ha^{-1}\,h^{-1}}$ in 2023 to 3,722 [2,484-4,884] $\mathrm{MJ\,mm\,ha^{-1}\,h^{-1}}$ in 2014. In addition, group i included only 2011 and 2019, despite the difference between their median values differing by a factor 1.6 (3,444 [2,190-4,869] and 5,681 [3,765-7,377] $\mathrm{MJ\,mm\,ha^{-1}\,h^{-1}}$ respectively), thereby indicating the occurrence of strong spatial similarities between these two seasons (6.c). Furthermore, 2019 median value exceeded the pluriannual seasonal median by a factor of 2.1. Finally, apart from

https://doi.org/10.5194/egusphere-2025-6030
Preprint. Discussion started: 20 January 2026

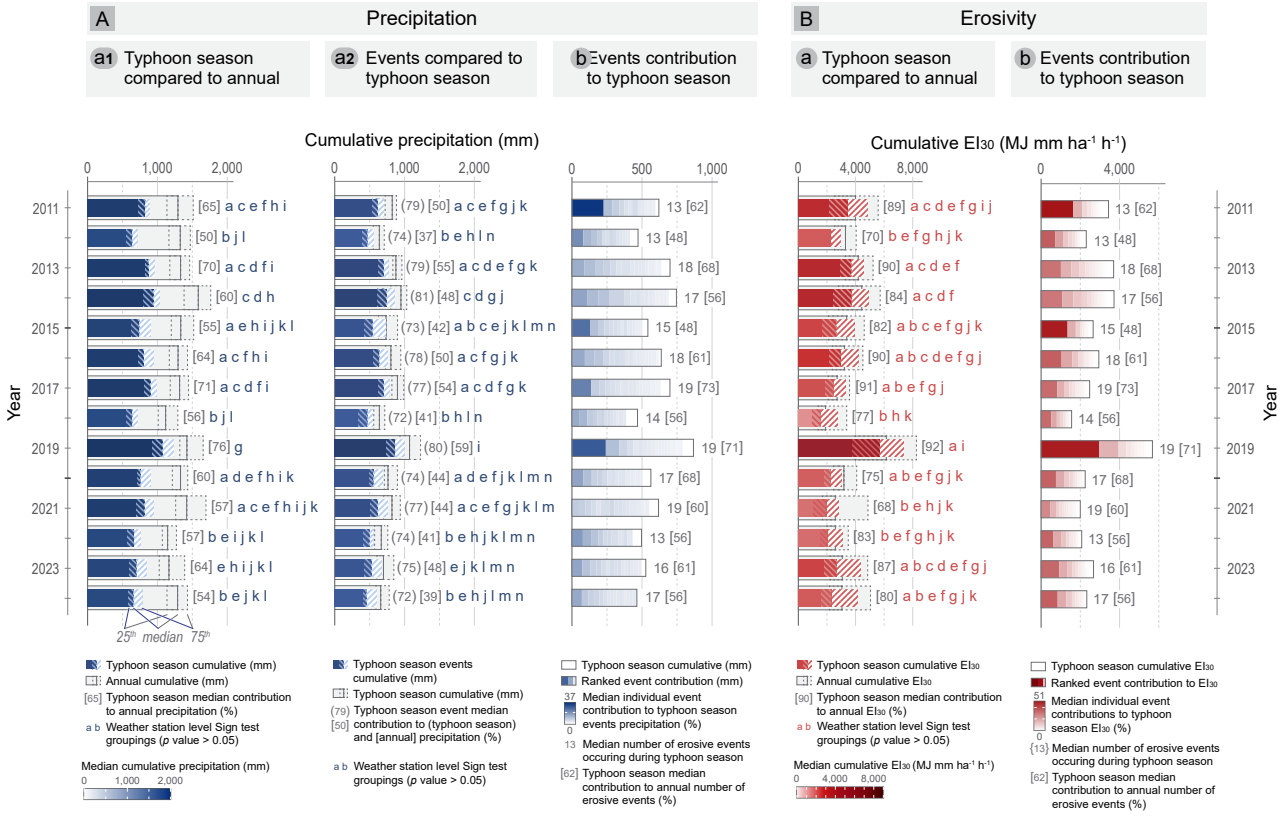

Figure 5. Annual summaries over the period 2011-2024 for [A] precipitation and [B] rainfall erosivity during (a) the typhoon season (June-October) (median, 25th and 75th quantiles), with station-level sign test groupings (p value $\geq$ 0.05), together with (b) ranked erosive event contribution (in %) to typhoon season cumulative median. Data was compiled for 58 weather stations located within a 110 km radius region around FDNPP.

those years with low seasonal value (2012, 2018, 2021, 2022), all years - including the highly erosive years such as 2019 - were classified within group a, suggesting a broadly similar spatial distribution of rainfall erosivity during these five months at the station scale despite the magnitude of interannual variability.

Seasonal precipitation (from June to October) represented a pluriannual median of 793 [665-944] mm and a mean of 820 $\pm$ 224 mm, both accounting for about 60 % of annual totals (Fig. 5.A.a). Seasonal median cumulative values ranged from 640 [552-711] mm in 2012 or 2018 to 1,075 [937-1,234] mm in 2019, with relative contribution to annual values ranging from 72 % in 2024 to 80 % in 2019. The sign-test groupings were more scattered than at the annual scale, indicating greater spatial heterogeneity in seasonal precipitation patterns. Most groups included six to seven years (e.g., a, c, e, f, h, j, k, and l). However, three smaller groupings: b, c, and d (with c and d differing by the inclusion of 2016 and 2021 in group c, and 2020 in group d), distinguished years with lower (2012, 2018, 2022, 2024) and higher (2011, 2013, 2014, 2016, 2017, 2020, 2021)

https://doi.org/10.5194/egusphere-2025-6030
Preprint. Discussion started: 20 January 2026

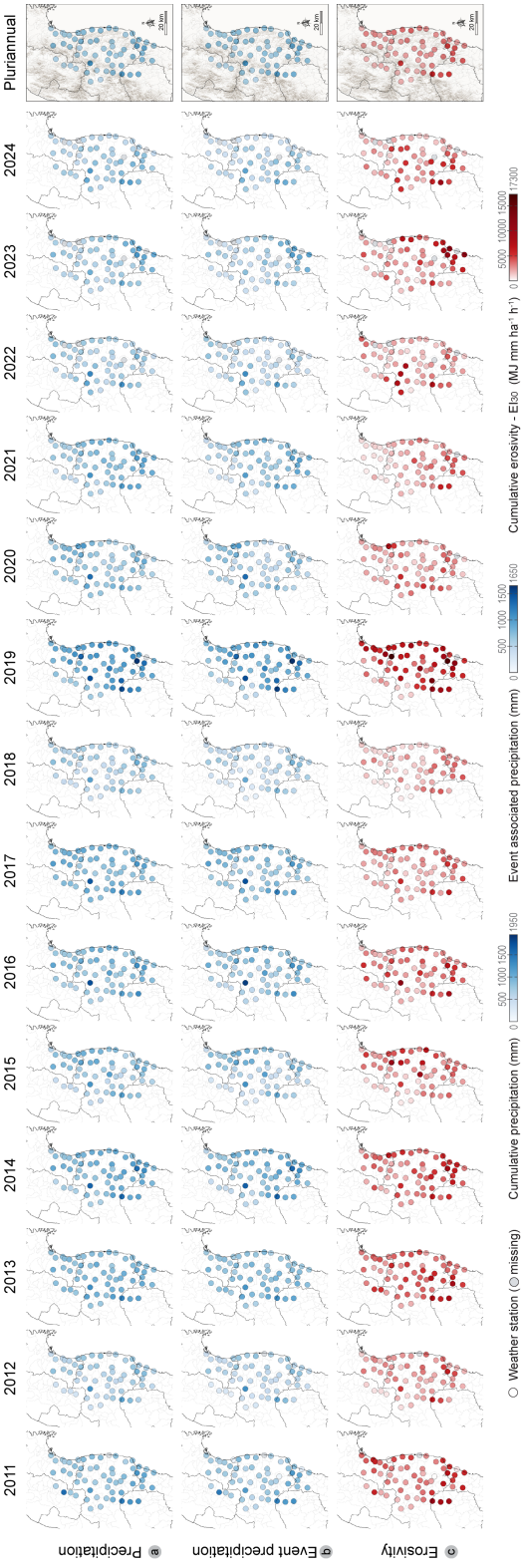

Figure 6. Annual records and pluriannual median values of typhoon season (June–October) cumulative (a) precipitation, (b) event-related precipitation, and (c) rainfall erosivity over 2011–2024 across 58 weather stations within a 110-km radius region around FDNPP.

https://doi.org/10.5194/egusphere-2025-6030
Preprint. Discussion started: 20 January 2026

seasonal totals. Moreover, group g only included 2019, which was the higher seasonal value of 1,075 [937-1,234] mm, being 1.4 times higher than the pluriannual seasonal median.

When considering only precipitation related with erosive events, median and mean seasonal values were 602 [474-749] mm and 626 ± 217 mm, respectively, corresponding to about 75 % of seasonal and 46 % of annual cumulative precipitation. The event-related precipitation ranged from 464 [409-604] mm in 2024 to 868 [740-997] mm in 2019. The relative contributions of these events to seasonal and annual cumulated precipitation ranged, respectively, from 72 % in 2024 to 81 % in 2014 and from 37 % in 2012 to 59 % in 2019. The statistical groupings of years were even more scattered in this case (Fig. 5.A.b), suggesting that precipitation related to erosive events exhibited more complex spatial and temporal variability than when considering total precipitations (Fig 6.a and b). While a few large groups (e, j, k) included up to nine years, smaller and overlapping groups became more common (four to six years), reflecting nuanced similarities and dissimilarities among years. For instance, 2012, previously included in three groups, was now found in five groups. Yet, lower-precipitation years (b, h, m, n) could still be distinguished from higher-precipitation years (a, c, d, f, g), although the large number of groups indicated some spatial variability between theses years (Fig. 6.b). In addition, 2019 again formed a distinct group (i), with a median event-related precipitation of 868 [740-997] mm, being 1.4 times higher than the pluriannual seasonal median.

At the annual scale, rainfall erosivity and total precipitation exhibited a moderate positive correlation at the station level (r^2 = 0.47) (n = 795; Fig. 7.a). However, when restricting the analysis to precipitation associated with erosive events only, the correlation increased to r^2 = 0.61 (n = 795), reflecting a better relationship between event-related precipitation and erosivity. A comparable pattern was observed for the June-October period, with correlation coefficients of r^2 = 0.62 for total seasonal precipitation and r^2 = 0.63 when considering only precipitation associated with erosive events (n = 795; Fig. 7.b).

3.2.2 Event-scale contribution

Although the June to October period concentrated most of the erosive events, precipitation, and rainfall erosivity, the number of such events showed no significant correlation with total seasonal precipitation (r^2 = 0.48), seasonal event-associated precipitation (r^2 = 0.53), or rainfall erosivity (r^2 = 0.18) at the station level (n = 795). This lack of correlation suggests that interannual variations in seasonal erosivity were primarily controlled by the intensity and characteristics of individual events rather than by their frequency.

In fact, during most years, a few high-intensity events accounted for a disproportionate share of the total seasonal rainfall erosivity (Fig. 5.A.c and B.c). Over the study period, the three most erosive events contributed individually, in median, 28, 14, and 9 % of annual erosivity, equivalent to 35, 17, and 11 % of seasonal erosivity. Their respective median rainfall erosivity were 912, 443, 278 $\mathrm{MJ\,mm\,ha^{-1}\,h^{-1}}$, associated with median precipitation amounts of 94, 62, and 49 mm (Appendix Table A9). In addition, the uppermost and the three most erosive events displayed a high correlation between precipitation and rainfall erosivity, of r^2 = 0.61 and 0.68 (n = 790), respectively (Fig. 7.c and d).

https://doi.org/10.5194/egusphere-2025-6030
Preprint. Discussion started: 20 January 2026

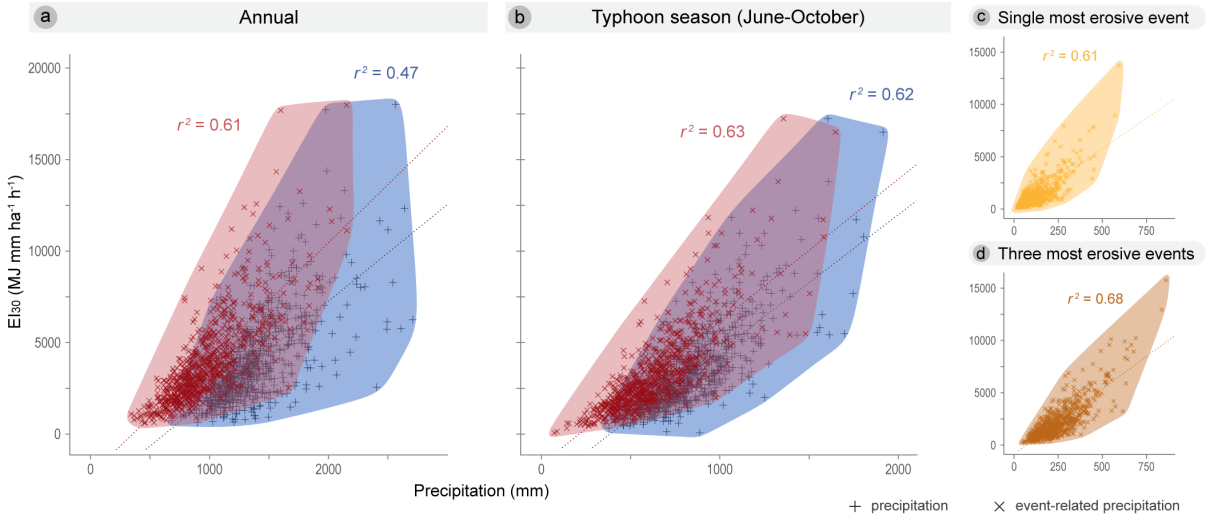

Figure 7. Relationship between rainfall erosivity (R-factor) and overall precipitation (blue x) or event related precipitation (red +) at the (a) annual scale (n = 795), (b) the scale of the typhoon season (June-October) (n = 795), during (c) the single most (EI_{30}; n = 790) and (d) the three most erosive events (n = 790) of each typhoon season for 58 weather stations over 2011-2024. 'r^2' indicates multiple squared Pearson linear correlation from fitted linear model.

These three most erosive events contributed cumulatively 55 % and 67 % of annual and seasonal erosivity, respectively. This corresponds to a cumulative median rainfall erosivity of 1,753 [1,106-2,744] $\mathrm{MJ\,mm\,ha^{-1}\,h^{-1}}$ and a mean of 2,208 ± 1,704 $\mathrm{MJ\,mm\,ha^{-1}\,h^{-1}}$. Their contribution varied across years, from 36 % (53 %) in 2021 to 58 % (63 %) in 2016 and 2017, and more exceptionally up to 65 % (79 %) in 2015, 67 % (77 %) in 2021, and 68 % (76 %) in 2019 (Appendix Table A9).

In terms of rainfall amount, these three events showing the highest erosivity represented a smaller proportion of the total seasonal and annual values, with median contributions of about 38 % and 17 %, respectively. Further, these values corresponded to 224 [170-305] mm in median and 247 ± 113 mm in mean cumulative precipitation. Their relative contribution to total annual (and seasonal) values varied moderately over the period, ranging from 11 % (27 %) in 2021 to 21 % (38 %) in 2017, and more exceptionally reaching 26 % (53 %) in 2011 and 27 % (47 %) in 2019.

The sign test showed similar groupings between their event-related precipitation and rainfall erosivity. Groupings were relatively scattered, with fourteen and eleven groups for erosivity and precipitation, respectively. Most groups encompassed nine to eleven years (e.g., e, j, k for erosivity; a, b, e, f, g, j for precipitation), reflecting high interannual variability. Years characterised by lower event erosivity and precipitation were generally clustered in distinct groups (h, k and b, d, h, l, n), whereas higher-intensity years were merged in c, d, i and a, c, f groups, respectively. The year 2015 appeared in both low- and high-intensity regimes (b, c, k and a, b, c, l, n). In contrast, 2011 and 2019 clearly stood out as from the high-intensity regime, being grouped together and alone for both precipitation (group a) and erosivity (group g). However, both years were also attributed to broader erosivity groups (e.g., a), which included several lower-intensity years, indicating that despite their exceptional magnitude,

https://doi.org/10.5194/egusphere-2025-6030
Preprint. Discussion started: 20 January 2026

2011 and 2019 shared some spatial similarities at the station level with the occurrence of less erosive events (Fig. 8).

When considering the single most erosive event of each season, it generated a median and mean rainfall erosivity of 912 [518-1,602] $\mathrm{MJ\,mm\,ha^{-1}\,h^{-1}}$ and 1,287 ± 1,243 $\mathrm{MJ\,mm\,ha^{-1}\,h^{-1}}$, respectively (Appendix Table A10). The relative contribution of this dominant event varied considerably among years, ranging from 24 % of annual values and 28-32 % of seasonal values in 2014 and 2018, to 30 % and 34 % in 2016, and more exceptionally up to 38 % and 46 % in 2015, to 44 % and 48 % during both 2011 and 2019. The most erosive event recorded in 2019 generated a median of 2,968 [1,545-3,926] $\mathrm{MJ\,mm\,ha^{-1}\,h^{-1}}$ from 241 [193-302] mm of precipitation, while the 2011 event reached 1,643 [1,149-2,562] $\mathrm{MJ\,mm\,ha^{-1}\,h^{-1}}$ from 226 [158-258] mm, and the 2015 event reached 1,350 [609-1,569] $\mathrm{MJ\,mm\,ha^{-1}\,h^{-1}}$ from 131 [100-166] mm. Nonetheless, the 2015 event did not markedly differ from other erosive years (e.g., 2014, 2016, 2023), and its grouping with 2011 and 2019 likely reflected differences in the spatial distribution of precipitation rather than its intensity alone (Fig. 9.b).

In terms of precipitation, these most erosive events represented a smaller proportion of cumulative precipitation, contributing in median 16 % and 7 % of seasonal and annual precipitation, respectively. This corresponded to a median precipitation of 94 [58-156] mm and a mean of 118 ± 83 mm. The relative contribution of these events to annual and seasonal precipitation varied from 4 % and 9 % in 2021 to 8 % and 13 % in 2013. More exceptionally, in 2015 and 2017, this contribution reached 10-11 % and 20-24 %, respectively, while 2011 and 2019 stood out with the highest contributions, 15 % and 32 % in 2011 to 16 % and 29 % in 2019, respectively.

The sign tests showed consistent patterns although scattered groupings for precipitation (thirteen groups) and erosivity (nine groups), confirming the strong interannual variability. Nonetheless, a large number of groups included between nine and twelve years for precipitation (b, c, d, f, g, i, k, l, m) and between ten and thirteen for erosivity (b, c, d, e, i), highlighted common event characteristics. In contrast, 2011 and 2019 formed distinct, isolated groups in precipitation (a) and erosivity (a and g). Conversely, 2015 occupied an intermediate position, overlapping with both high- and moderate-intensity regimes (c-g, l for precipitation; a-e, i for erosivity), suggesting the occurrence of spatially heterogeneous conditions (Fig. 9.b).

Regarding the spatial distribution of the most erosive events, these heavy storms were generally observed in the southern part of the study area (e.g. Hanazono, Nasukougen, Ootawara, Kuroen, Hitachi) or in the central area (e.g. Ishakawa, Hippo, Nihonmatsu, Kawauchi, Washiku-ra), and more exceptionally in the northern area (e.g. Shinchi, Natori) (Fig. 9.b, Appendix Table A10). For several years, both the three most erosive events and the single most erosive event, were recorded at the same weather stations, such as Hanazono in 2012, Shinchi in 2014 and 2020, Washikura in 2016, Hippo in 2019, and Hitachi in 2023 (Appendix Table A9 and A10). Apart from 2019, the other years were generally years with lower erosivity. Furthermore, in 2011, 2015 and 2015 the annual highest erosive event maxima were recorded in the central-northern part of the area (i.e., Natori and Hippo), while when considering the three most erosive events in 2011 and 2015, the stations

https://doi.org/10.5194/egusphere-2025-6030
Preprint. Discussion started: 20 January 2026

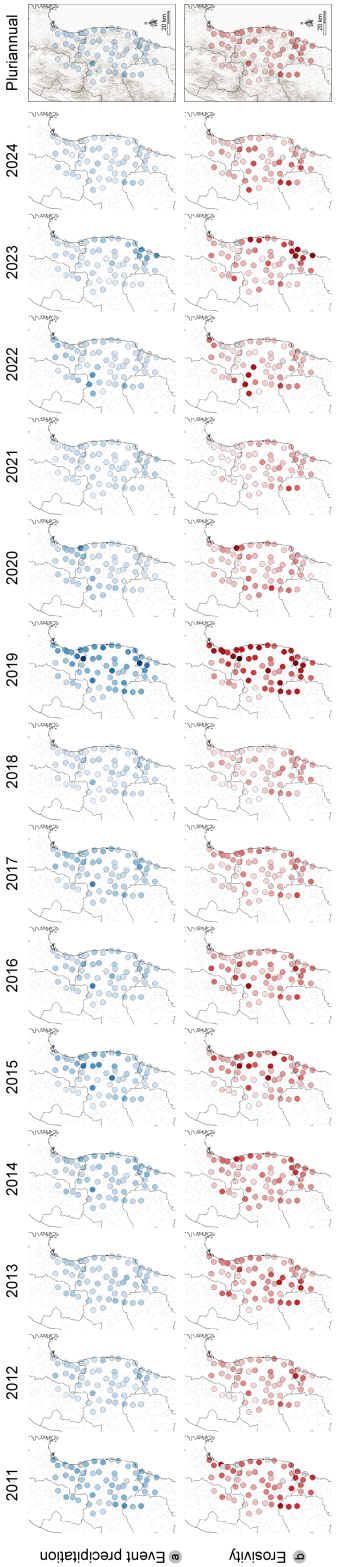

Figure 8. Annual records and pluriannual median values of the three most erosive event (a) related precipitation and (b) rainfall erosivity over the period 2011-2024 across the 58 weather stations located within a 110-km radius region around FDNPP.

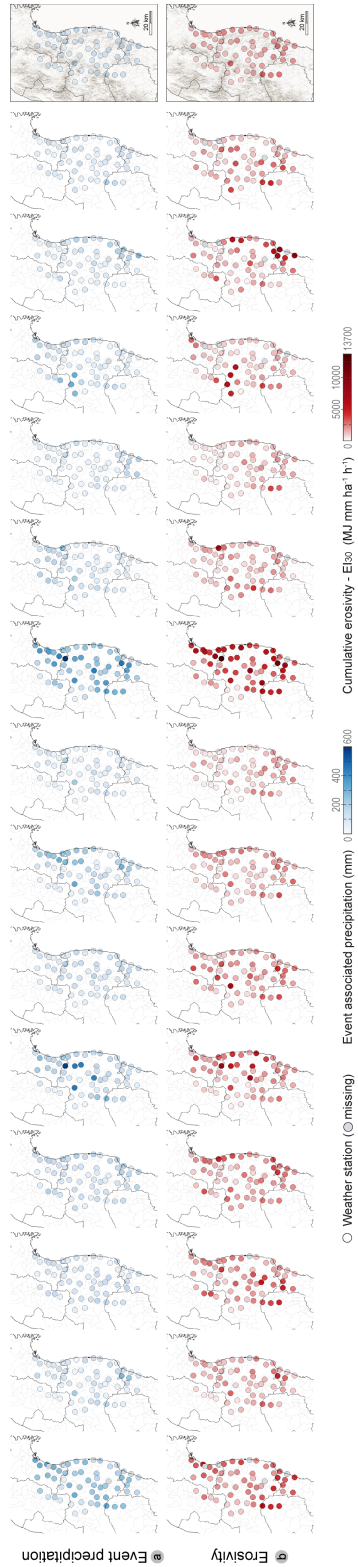

Figure 9. Annual records and pluriannual median values of the single most erosive event (a) related precipitation and (b) rainfall erosivity over the period 2011-2024 across the 58 weather stations located within a 110-km radius region around FDNPP.

https://doi.org/10.5194/egusphere-2025-6030
Preprint. Discussion started: 20 January 2026

where they were recorded were located in the southern area (i.e., Nasukougen, Kawauchi). For both the single most and the three most erosive events, in 2019, the Hippo station recorded the absolute maximum erosivity of the entire period, reaching 13,690 $\mathrm{MJ\,mm\,ha^{-1}\,h^{-1}}$ (594 mm) and 15,761 $\mathrm{MJ\,mm\,ha^{-1}\,h^{-1}}$ (860 mm), respectively (Fig. 8.b and 9.b).

4 Discussion

4.1 Magnitude and annual variability of precipitation and erosivity

At the annual scale, precipitation and rainfall erosivity exhibited significant interannual variability throughout the study period (2011-2024). Across the 110 km radius region around the FDNPP distributed among the eastern part of Fukushima Prefecture, the southern part of Yamagata and Miyagi Prefectures, and the northern part of Tochigi and Ibaraki Prefectures, the median and mean annual precipitation across the 58 stations ranged from 1,119 to 1,581 $\mathrm{mm\ yr^{-1}}$, which is consistent with the regional climatology of the Tōhoku region (Kim et al., 2010; Duan et al., 2015; Laceby et al., 2016a). However, the 2011-2024 annual mean (1,360 $\pm$ 301 $\mathrm{mm\ yr^{-1}}$) was about 4 % lower than the long-term mean reported by (Laceby et al., 2016a) for 1979-2015 (1,420 $\pm$ 235 $\mathrm{mm\ yr^{-1}}$).

Rainfall erosivity displayed comparatively larger variability than precipitation, with median annual values ranging from 1,908 to 6,159 $\mathrm{MJ\,mm\,ha^{-1}\,h^{-1}\,yr^{-1}}$, which was consistent with ranges of values reported by previous studies. Shiono et al. (2013) modelled a mean annual range of 2,500-7,500 $\mathrm{MJ\,mm\,ha^{-1}\,h^{-1}\,yr^{-1}}$, while Yamaguchi et al. (2014) and Laceby et al. (2016a) reported values comprised between 1,866-7,159 $\mathrm{MJ\,mm\,ha^{-1}\,h^{-1}\,yr^{-1}}$ and 1,986-4,217 $\mathrm{MJ\,mm\,ha^{-1}\,h^{-1}\,yr^{-1}}$, respectively. However, the mean annual erosivity over 2011-2024 (3,881 $\pm$ 2,320 $\mathrm{MJ\,mm\,ha^{-1}\,h^{-1}\,yr^{-1}}$) exceeded previous estimates of Yamaguchi et al. (2014) by 15 % over 2001-2011 (3,366 $\mathrm{MJ\,mm\,ha^{-1}\,h^{-1}\,yr^{-1}}$; 23 stations) and by 5 % Laceby et al. (2016a) over 1995-2015 (3,696 $\pm$ 1,327 $\mathrm{MJ\,mm\,ha^{-1}\,h^{-1}\,yr^{-1}}$; 42 stations), despite the fact that similar areas were considered in these investigations. Yoshimura et al. (2015), estimated rainfall erosivity between July 2011 and November 2012 across four sites in Kawamata Town (Fukushima Pref., central-west part) as ranging between 2,783-4,107 $\mathrm{MJ\,mm\,ha^{-1}\,h^{-1}\,yr^{-1}}$, which is consistent with annual total values recorded in 2011 and 2012 (median: 3,884 [2,341-5,556] and 3,303 [2,531-4,049] $\mathrm{MJ\,mm\,ha^{-1}\,h^{-1}\,yr^{-1}}$; mean: 4,150 $\pm$ 2,326 and 2,308 $\pm$ 1,903 $\mathrm{MJ\,mm\,ha^{-1}\,h^{-1}\,yr^{-1}}$). This result is consistent with that of previous works, as both rainfall and erosivity were shown to exhibit strong interannual fluctuations, as indicated by large SD or IQR values (Shiono et al., 2013; Laceby et al., 2016a). In this context, the use of median values thus provide a more robust representation than mean values, as they are less sensitive to skewed distributions. Nonetheless, some increase in total cumulated values likely reflects the growing influence of recent high-intensity events, increasing annual total values during the most recent period (e.g. 2015 and 2019).

These observations align with climate projections for Tōhoku region, and broader Japan, showing the occurrence of a climatic transition from humid continental (Dfa/Dfb) to humid subtropical (Cfa) conditions (Beck et al., 2018). Future projections indicate a slight decrease in mean annual precipitation in the coming decades (Kim et al., 2010; Hatsuzuka and Sato, 2019). However, both interannual variability and the intensity of high-precipitation events are expected to increase (Shiono et al.,

https://doi.org/10.5194/egusphere-2025-6030
Preprint. Discussion started: 20 January 2026

2013; Duan et al., 2015; Kawase et al., 2023; Suzuki et al., 2024). Although most projections show a decrease in monthly total precipitation and a lower frequency of extreme events, an increase in their cumulative precipitation is projected (Hatsuzuka and Sato, 2019; Kawase et al., 2023; Suzuki et al., 2024). Consequently, annual total precipitation or rainfall erosivity are likely becoming metrics that are less representative of the hydrological situation, as interannual variability and contrasts are becoming less driven by total precipitation and are instead becoming increasingly controlled by the frequency and characteristics of extreme precipitation events.

4.2 Seasonal concentration of precipitation and erosivity

Precipitation and rainfall erosivity were strongly concentrated in the summer months, from June to October, which were statistically distinct from the rest of the year. This was mainly observed because of the frequent occurrence of extreme events such as typhoons generating a high rainfall volume with a high erosivity during these months. Within this period, two subgroups could be distinguished: (i) the core typhoon season (July-September), accumulating most of the seasonal rainfall and erosivity, and (ii) the transition months (June and October), characterised by generally lower total rainfall although being occasionally characterised by the occurrence of heavy events (e.g. October 2019).

During these five months, a median of 16 erosive events occurred each year, representing about 61 % of the annual number of events. Although the event frequency was weakly related to total seasonal precipitation (r^2 = 0.48) or total rainfall erosivity (r^2 = 0.18), these events contributed disproportionately to annual erosivity values, accounting in median for 86 % (range: 70-93 %) of annual rainfall erosivity and, more moderately, for 46 % (range: 37-59 %) of annual precipitation. However, when considering all precipitation occurring during the season, the season contribution to the annual total reached 61 % (range: 50-76 %), among which precipitation associated with erosive events represented 76 % (range: 72-81 %) of seasonal precipitation. These results were consistent with those of Laceby et al. (2016a), who reported similar seasonal contributions (86 % of annual erosivity and 60 % of total precipitation) for the 1995-2015 period. In agreement with these results, correlations between total annual precipitation and erosivity were low (r^2 = 0.39 in Laceby et al., 2016a; r^2 = 0.47 in this study), although they increased significantly when restricted to precipitation associated with erosive events at the annual scale (r^2 = 0.61) or when considering the typhoon season only (r^2 = 0.62-0.63). This reinforces the importance of considering event-related and/or seasonal precipitation when estimating rainfall erosivity in regions dominated by extreme precipitation dynamics such as that of Fukushima Prefecture.

Furthermore, the typhoon season showed a substantial interannual variability associated with rainfall erosivity and precipitation, with median seasonal erosivity ranging from 1,560 to 5,681 $\mathrm{MJ\,mm\,ha^{-1}\,h^{-1}}$ and precipitation ranging from 640 to 1,075 mm or from 464 to 868 mm when considering event-related precipitation only. These ranges were consistent with the seasonal erosivity estimates provided by Shiono et al. (2013) for June-August and September-November (each 1,000-2,500 $\mathrm{MJ\,mm\,ha^{-1}\,h^{-1}}$; cumulative 2,000-5,000 $\mathrm{MJ\,mm\,ha^{-1}\,h^{-1}}$). Projections by the same authors for 2031-2050 suggest increases of 0-50 % in summer and 50-100 % in autumn erosivity, which are already comparable to those recorded during several recent years showing local maxima of about 11,000 $\mathrm{MJ\,mm\,ha^{-1}\,h^{-1}}$ (2011, 2015, 2016, 2023), although these remained

https://doi.org/10.5194/egusphere-2025-6030
Preprint. Discussion started: 20 January 2026

below the 2019 maximum of 17,244 $\mathrm{MJ\,mm\,ha^{-1}\,h^{-1}}$. Comparisons with other studies remain limited, as most studies have focused on annual (Yamaguchi et al., 2014; Laceby et al., 2016a), monthly (Hatsuzuka and Sato, 2019; Suzuki et al., 2024), periodic (Yoshimura et al., 2015), or event scales (Chartin et al., 2017; Loa and Kawagoe, 2021).

4.3 Extreme erosive event dominance

Within the typhoon season, a large proportion of rainfall erosivity originated from a limited number of high-intensity events. Over the 2011-2024 period, the three most erosive events of each typhoon season accounted for a median of 67 % (range: 53-76 %) of the seasonal rainfall erosivity and 55 % of the total annual values, with interannual variations ranging from 36 % to 68 %. These events cumulatively generated a median rainfall erosivity of 1,753 [1,106-2,744] $\mathrm{MJ\,mm\,ha^{-1}\,h^{-1}}$ (mean = 2,208 ± 1,704 $\mathrm{MJ\,mm\,ha^{-1}\,h^{-1}}$) and precipitation of 224 [170-305] mm (mean = 247 ± 113 mm), corresponding to about 17 % of the annual precipitation. When considering the single most erosive event of each season only, its median contribution reached 35 % (range: 26-51 %) of the typhoon-season total and 28 % (range: 10-37 %) of annual rainfall erosivity, with a median erosivity of 912 [518-1,602] $\mathrm{MJ\,mm\,ha^{-1}\,h^{-1}}$ and a mean of 1,287 ± 1,243 $\mathrm{MJ\,mm\,ha^{-1}\,h^{-1}}$. In terms of rainfall, this dominant event accounted for about 8 % of annual precipitation (median = 94 [58-156] mm; mean = 118 ± 83 mm).

These contributions were consistent with those previously reported in the region. Laceby et al. (2016a) calculated that major tropical cyclones contributed 40 % of the annual rainfall erosivity (mean = 1,462 ± 637 $\mathrm{MJ\,mm\,ha^{-1}\,h^{-1}}$) and 22 % of the annual precipitation (mean = 422 mm) between 1995 and 2015. The slightly higher contributions to annual erosivity found in the current research for the most erosive events likely result from the higher values observed between 2015 and 2024 as well as from potential methodological differences, as our approach identified events statistically among all erosive rainfall events rather than focusing exclusively on tropical cyclones. This broader definition allows the inclusion of intense events that did not coincide with typhoon events that may occasionally generate comparable rainfall erosivity levels.

Nonetheless, the magnitude of the most erosive events identified in the current study aligns well with previous estimates for individual typhoons. Chartin et al. (2017) reported rainfall erosivity values for the main typhoon of each year between 2011 and 2015. The mean erosivities reported by Chartin et al. (2017) for the Roke typhoon in 2011 (ID-1105) (1,695 ± 1,066 $\mathrm{MJ\,mm\,ha^{-1}\,h^{-1}}$, 39 stations) and the Etau typhoon in 2015 (ID-1518) (1,581 ± 1,577 $\mathrm{MJ\,mm\,ha^{-1}\,h^{-1}}$, 40 stations) were comparable to the values obtained here for the most erosive events of the same years (2011: 1,929 ± 1,098 $\mathrm{MJ\,mm\,ha^{-1}\,h^{-1}}$, 53 stations; 2015: 1,617 ± 1,449 $\mathrm{MJ\,mm\ ha^{-1}\,h^{-1}}$, 58 stations). Loa and Kawagoe (2021) investigated Typhoon Hagibis in 2019 (ID-1919) using 60 min precipitation data, and reported mean values of 2,354 $\mathrm{MJ\,mm\,ha^{-1}\,h^{-1}}$ within the Abukuma catchment and local maxima exceeding 10,000 $\mathrm{MJ\,mm\,ha^{-1}\,h^{-1}}$ in its northern part, which remains in the same range of values as the mean value calculated over the entire region (3,135 ± 2,297 $\mathrm{MJ\,mm\,ha^{-1}\,h^{-1}}$) and which is consistent with the local maximum measured at Hippo station (13,690 $\mathrm{MJ\,mm\,ha^{-1}\,h^{-1}}$), close to the northern part of the Abukuma catchment.

In contrast, the mean erosivity values reported by Chartin et al. (2017) for the main events that occurred in 2012 (Jelawat) and 2013 (Wipha & Francisco; ID-1326) (262 ± 197 $\mathrm{MJ\,mm\,ha^{-1}\,h^{-1}}$, 36 stations; and 549 ± 317 $\mathrm{MJ\,mm\,ha^{-1}\,h^{-1}}$, 39 stations) were significantly lower than those obtained in the current research (928 ± 707 and 1,311 ± 854 $\mathrm{MJ\,mm\,ha^{-1}\,h^{-1}}$).

https://doi.org/10.5194/egusphere-2025-6030
Preprint. Discussion started: 20 January 2026

For 2014, which included two major typhoons (Phanfone & Vongfong; ID-1418 and 1419), Chartin et al. (2017) reported cumulative mean erosivity values (1,034 ± 759 $\mathrm{MJ\,mm\,ha^{-1}\,h^{-1}}$, 40 stations) slightly lower although remaining within the standard deviation of the corresponding most erosive events identified here (1,198 ± 670 $\mathrm{MJ\,mm\,ha^{-1}\,h^{-1}}$, 58 stations). These differences likely reflect methodological differences in the identification of dominant erosive events, particularly during years characterised by high spatial variability or by the occurrence of multiple events of similar intensity. In this study, the primary objective was to assess major interannual trends and similarities, and to compare the relevance of annual versus seasonal scales for deriving representative erosivity metrics. Nevertheless, a more detailed characterisation of the succession of erosive events within each year, and at the regional scale, would be also valuable. Such an approach, however, presents methodological challenges, since individual events do not start simultaneously across the entire study area and may differ substantially in spatial extent and intensity, as highlighted on multiple occasions throughout this work. In addition, while typhoons were often highlighted and studied other precipitation events, such as low-pressures events or linear precipitation bands (線状降水帯 - senjo kousuitai in Japanese), were also reported to generate exceptionally high cumulative precipitation (JMA, 2025). However, these events are less reported as international level although being listed (https://www.bousai-top.com/, in Japanese) and studied in Japan (Nishii). Therefore, developing an approach without any preconceptions about the nature of the event could be appropriate.

The years 2011 and 2019 consistently emerged as the most erosive of the study period, with 2019 standing out across all metrics, with the occurrence of typhoon Roke and Hagibis. Although 2015 appeared less remarkable when considering annual or seasonal total precipitation, its most erosive event (Etau), showed statistical similarities with those of 2011 and 2019. In the literature, these three events were often reported as the most impactful during the period since Fukushima accident (Chartin et al., 2017; Evrard et al., 2020; Vandromme et al., 2023; Chalaux-Clergue et al., 2024b). Notably, during each of these years, the most erosive event alone accounted for 46-48 % of the seasonal erosivity and 44 % (2011 and 2019) to 38 % (2015) of the annual total values, whereas in other years, the most erosive events typically contributed 26-35 % of the seasonal and 24-30 % of the annual erosivity. This recurrent pattern, where a single event dominates the seasonal erosivity with a similar relative magnitude despite contrasting seasonal or annual total values, highlight the similarities of these exceptional typhoons.

Nevertheless, the use of the R-factor or EI_{30}, presents limitations, particularly with regard to its direct relationship with river sediment transport in steep, mountainous environments, such as those found in Japan, which differ significantly from the conditions in which it was developed (Wischmeier and Smith, 1958). Although the R-factor was developed to reflect the impact of erosive rainfall on sheet and rill erosion on hillslopes, it was not directly designed to account for complex processes such as gully erosion and mass movement events (e.g. landslides and debris flows), which occur in the Fukushima region (Vandromme et al., 2023). Consequently, although the R-factor and EI_{30} allow comparison between events or periods, their direct use to characterise the soil erosion and sediment transport in such steep and geomorphologically active regions requires careful consideration and necessitates complementary modelling approaches.

https://doi.org/10.5194/egusphere-2025-6030
Preprint. Discussion started: 20 January 2026

4.4 Implication for sediment and ^{137}Cs dynamics

The river systems draining the eastern part of Fukushima Prefecture have demonstrated their strong reactivity to intense rainfall events (Chartin et al., 2013; Evrard et al., 2014, 2020). Since 2011, sediment and ^{137}Cs transfers in this region have mainly occurred during a limited number of events, corresponding mainly to tropical storms and typhoons (Osawa et al., 2018; Yamashiki et al., 2014; Kitamura et al., 2016), that exceeded regional erosivity thresholds was estimated to range between 60 and 100 mm (Evrard et al., 2014). These major events were identified as the main drivers of most of the annual sediment and radiocesium exports (Yamashiki et al., 2014; Sakaguchi et al., 2015; Iwagami et al., 2017; Osawa et al., 2018). According to the intensity of the events and generated runoff volumes, the eroded material can be temporary stored within the river system and remobilised by the following events (Golosov et al., 2022). Strong erosive rainfall events were also shown to generate a high sediment connectivity pattern across the landscape, which may occasionally connect regions that are distant from the river system (Chartin et al., 2017), such as forested land that may supply a perennial source of contaminated material to river systems (Laceby et al., 2016b; Huon et al., 2018; Chalaux-Clergue et al., 2024b). However, not all extreme events necessarily lead to high ^{137}Cs exports. Deep-rill or gully erosion may predominantly mobilise subsurface layers that are less contaminated than the topsoil as they were sheltered from the initial atmospheric radioactive fallout (Oda et al., 2022; Vandromme et al., 2023). In addition, seasonal factors such as the density of the vegetation cover or the soil antecedent moisture may modulate erosion intensity, with typhoons occurring during full canopy conditions being less erosive than those occurring during early spring or late in autumn (Yoshimura et al., 2015). Nevertheless, since few extreme events occur in the late-autumn or winter months, the risk of severe contamination transfers through erosion outside of the typhoon season appears to remain limited.

Over the longer term, the supply of contaminated sediment to river systems has gradually decreased due to past successive erosive exports or decontamination and, to a lesser extent following the physical decay of ^{137}Cs, reducing the inventory of potential contaminated material (Osawa et al., 2018; Taniguchi et al., 2019). In parallel, the large-scale decontamination of farmland has removed contaminated material from locations that are highly connected to the river system (Chartin et al., 2017; Vandromme et al., 2023). Accordingly, the ^{137}Cs activity measured in river sediments continuously decreased by 90 % between 2011 and 2020 (Yoshimura et al., 2015; Taniguchi et al., 2019; Evrard et al., 2020). Nonetheless, according to Ueda et al. (2021), only a limited proportion of the initial ^{137}Cs deposited has been flushed away to the Pacific Ocean through the rivers by 2021. In fact, 12 years after the accident, about 67 % of the initial ^{137}Cs was still stored under forests, which cover about 80 % of landscapes in the region (Onda et al., 2020; Vandromme et al., 2023). As a consequence, forests may act as persistent source of ^{137}Cs intermittently supplying contaminated material during intense storms to river systems (Huon et al., 2018; Vandromme et al., 2023; Chalaux-Clergue et al., 2024b). In addition, under the increased occurrence of extreme events, the evolution of water reservoir dam management practices may impact the sediment accumulation and their downstream propagation (Chalaux-Clergue et al., 2024b; Hazet et al., 2025). For instance, as discussed in Chalaux-Clergue et al. (2024b), large water releases during the 2015 and 2019 events observed at the Mano Dam Reservoir, likely reduced reservoir sediment trapping efficiency during such events, and likely facilitated the downstream export of both sediment and ^{137}Cs.

https://doi.org/10.5194/egusphere-2025-6030
Preprint. Discussion started: 20 January 2026

Projected changes in regional climate will likely impact sediment and contaminant dynamics across the landscape. As discussed earlier, fewer but more intense rainfall events are expected to occur in the coming decades (Hatsuzuka and Sato, 2019; Kawase et al., 2023; Suzuki et al., 2024). This may modify sediment residence times and release along the river system and sediment connectivity across landscapes. The combination of increasing erosivity and longer dry periods could also favour slope destabilization, wildfires, or drought-induced soil degradation, which may then enhance the potential for contaminated sediment mobilisation during erosive events (Evrard et al., 2023). These evolving conditions underline the importance of maintaining long-term sediment and river monitoring, and integrating event-scale variability into risk assessments for contaminated catchments.

Finally, the precipitation and rainfall erosivity datasets produced in this study provide an updated characterisation of precipitation and erosivity metrics around the FDNPP area over the 2011 to 2024 period. This could support future research on sediment and ^{137}Cs transfers in the Fukushima region. Following the approach of Laceby et al. (2016a), this dataset could be used to generate annual, monthly and event-scale *R*-factor maps through spatial interpolation at the regional scale, which could then provide an improved basis for modelling studies of sediment and radiocesium dynamics. The datasets are freely available on Zenodo. However, given the complex mountainous context of the region, with a pronounced topographic variability, spatial interpolation of point-based station data is complex and may present limitations (e.g., R^2 ranging from 0.56-0.86 in Laceby et al., 2016a and 0.83-0.95 in Chartin et al., 2017) (Page et al., 2022). In this context, the increasing accessibility of radar-based precipitation products, which, currently offers spatial resolutions down to 1 km^2 and temporal resolutions of 5 min, along with weather station data, offers promising perspectives to enhance such analyses (Turini et al., 2021; Cremonini et al., 2023; Palarz et al., 2024). These data would enable high-resolution, spatially explicit assessments of regional climatology (Fairman et al., 2015) and precipitation and rainfall erosivity patterns from event to annual scales (Auerswald et al., 2019).

5 Conclusions

The precipitation and rainfall erosivity were analysed within a 110 km radius region around the Fukushima Dai-ichi Nuclear Power Plant (FDNPP), using 10-minute precipitation data from 58 JMA weather stations covering the period from January 2011 to December 2024. Precipitation and erosivity dynamics were examined and compared at annual, monthly, and seasonal scales, and the characteristics of the uppermost and three most erosive events of each year were investigated.

The median annual precipitation amounted to 1318 mm, including a contribution of 917 mm from erosive events associated with an erosivity of 3290 $\mathrm{MJ\,mm\,ha^{-1}\,h^{-1}}$, and marked with interannual variability. However, 61 % of erosive events (16 events) occurred between June and October, accounting for 46 % of annual precipitation (602 [474-749] mm) and 86 % of annual erosivity (2,698 [1,826-4,076] $\mathrm{MJ\,mm\,ha^{-1}\,h^{-1}}$). The typhoon season (June-October) statistically stood out and appeared to be the most relevant temporal scale for conducting regional analyses of precipitation and rainfall erosivity (r^2 = 0.62) and should be preferred to the annual scale (r^2 = 0.47). However, at both annual and seasonal scales, considering only precipitation associated with erosive events also provided a consistent framework (r^2 = 0.61 and 0.63, respectively). Nevertheless, most of

https://doi.org/10.5194/egusphere-2025-6030
Preprint. Discussion started: 20 January 2026

the annual erosivity was generated by a limited number of events. The three most erosive events contributed, in median, 55 % of the annual total (1,753 [1,106-2,744] $\mathrm{MJ\,mm\,ha^{-1}\,h^{-1}}$; 224 [170-305] mm), while the single most erosive event alone accounted for 28 % (912 [518-1,602] $\mathrm{MJ\,mm\,ha^{-1}\,h^{-1}}$; 94 [58-156] mm). Exceptional years, such as 2011, 2015, and 2019 were particularly dominated by a single event, which contributed up to 38-44 % of annual erosivity.

In over a decade since the accident, the region nearby the FDNPP has remained exposed to major erosive events, which continue to drive sediment and radiocesium redistribution. A more detailed characterisation of the spatial and temporal dynamics of these events, supported by spatially-distributed data, such radar-based rainfall products, should enhance our understanding of their local variability and impact. Ongoing climate change, which is likely to increase the intensity of extreme events and to raise disturbances, such as droughts and wildfires, could further increase soil disturbance and sediment transfers. This highlights the need for sustained observation and modelling at regional and event scales.

Code and data availability. Raw precipitation records from the 58 JMA weather stations used in this study, along with all derived datasets, are available on Zenodo (https://doi.org/10.5281/zenodo.17573969) (Chalaux-Clergue et al., 2025)). The derived datasets include station-level (i) the characteristics of all identified rainfall erosive events, and (ii) station-level annual and pluriannual metrics, over annual, monthly, and typhoon season period, as well as metrics for the single most and the three most erosive events. The R Markdown (Rmd) file, encompassing the code for precipitation analysis, metric calculation, and plot generation, is available in the Supplement. The functions developed to identify precipitation events and compute their specific characteristics (including start and end date-time, duration, cumulative precipitation, I_{30}, and EI_{30}) were compiled within the R package RainErosivity (version 1.1.0; Chalaux-Clergue, 2025). This package is freely accessible on GitHub (https://github.com/tchalauxclergue/RainErosivity) and has been archived on Zenodo (https://doi.org/10.5281/zenodo.14745960).

https://doi.org/10.5194/egusphere-2025-6030
Preprint. Discussion started: 20 January 2026

Appendix A: Tables

Table A1. Annual summary of cumulative precipitation within a 110-km radius region around FDNPP over the period 2011-2024. Statistics are based on 10-min data from 58 weather stations (data from the Japanese Meteorological Agency). '25th' and '75th' indicate the 25th and 75th quantiles, respectively. 'SD' indicates standard deviation. Sign tests were performed on station-level values and 'Sign test group' indicates statistically undistinguishable groups with a p value ≥ 0.05. Regional statistics were calculated using station-level values including all years aggregated.

Year	Number of station	Cumulative precipitation (mm)									
		Median	25th	75th	Mean	SD	Sign test group	Local minimum		Local maximum	
								Name		Name	
2011	53	1296	1136	1512	1362	311	a, b, f, i	Inawashiro	1006	Kaminoyamasakayama	2709
2012	57	1328	1165	1471	1349	290	a, b, f, i	Inawashiro	934	Nasukougen	2194
2013	57	1332	1177	1462	1342	222	a, b, f, g, i	Yanagawa	988	Nasukougen	1953
2014	58	1584	1382	1763	1608	295	c, e, g	Shiogama	1140	Hanazono	2502
2015	58	1334	1199	1520	1381	251	a, b, f, g, i	Kaminoyamasakayama	1015	Washikura	2234
2016	58	1294	1170	1432	1344	272	a, b, f, g, i	Yanagawa	988	Washikura	2639
2017	58	1318	1183	1445	1360	273	a, b, f, g, i	Yanagawa	970	Washikura	2611
2018	58	1119	1012	1293	1162	249	d, h	Yanagawa	757	Washikura	2068
2019	57	1424	1322	1654	1521	326	c, e, f, g	Kaminoyamasakayama	1122	Hanazono	2566
2020	57	1331	1216	1434	1365	273	a, b, e, f, g, i	Tamakawa	915	Washikura	2494
2021	57	1420	1261	1696	1490	320	b, c, e, f, g	Yanagawa	970	Washikura	2404
2022	54	1146	1071	1272	1220	270	d, h, i	Yanagawa	836	Washikura	2236
2023	54	1164	1025	1391	1198	265	d, h, i	Natori	684	Hanazono	1898
2024	54	1289	1138	1431	1312	274	a, b, f, h, i	Yanagawa	890	Washikura	2182
Regional summary:		*1318*	*1148*	*1501*	*1360*	*301*	-	-	-	-	-

https://doi.org/10.5194/egusphere-2025-6030
Preprint. Discussion started: 20 January 2026

Table A2. Annual summary of cumulative precipitation within a 110-km radius region around FDNPP over the period 2011-2024. Statistics are based on 10-min data from 58 weather stations (data from the Japanese Meteorological Agency). '25th' and '75th' indicate the 25th and 75th quantiles respectively, 'SD' indicates standard deviation. Sign tests were performed on station-level values and 'Sign test group' indicates statistically undistinguishable groups with a p value ≥ 0.05. Number of months out of the theoretical maximum of 812. Regional statistics were calculated using station-level values with all years aggregated.

Month	Number of month	Cumulative precipitation (mm)											
		Median	25th	75th	Mean	SD	Sign test group	Local minimum			Local maximum		
								Name	Year		Name	Year	
January	789	43	18	76	55	46	a	Higashishirakawa	2019	0	Hanazono	2020	270
February	788	39	23	64	49	36	b	Hirono	2018	2	Hitachi	2014	188
March	792	86	54	130	94	54	c, d	Iwatama	2013	0	Hanazono	2018	380
April	791	96	70	128	105	48	c, d, e	Souma	2023	22	Hanazono	2013	377
May	791	99	74	138	111	60	d, e, i	Yanagawa	2013	18	Oonou	2012	536
June	795	122	80	178	137	75	f, i	Fukushima	2018	26	Washikura	2014	575
July	795	162	114	227	178	96	g	Taira	2016	15	Washikura	2020	622
August	795	133	90	212	159	102	h, i	Ishikawa	2012	10	Washikura	2016	932
September	795	170	123	238	191	98	g	Yamagata	2014	26	Hippo	2015	673
October	795	105	66	212	154	135	e, f, h, i	Souma	2015	0	Hippo	2019	902
November	795	58	36	83	65	42	j	Shiroishi	2020	0	Washikura	2023	250
December	779	49	27	82	62	51	j	Shirakawa	2020	0	Yonezawa	2014	366
Regional summary:		*92*	*52*	*150*	*114*	*90*	-	-	-	-	-	-	-

https://doi.org/10.5194/egusphere-2025-6030
Preprint. Discussion started: 20 January 2026

Table A3. Annual summary of cumulative rainfall erosivity (EI_{30} or *R*-factor) within a 110-km radius region around FDNPP over the period 2011-2024. Statistics are based on 10-min data from 58 weather stations (data from Japanese Meteorological Agency). '25_{th}' and '75^{th}' indicate the 25^{th} and 75^{th} quantiles, respectively. 'SD' indicates standard deviation. Sign tests were performed on station-level values and 'Sign test group' indicates statistically undistinguishable groups with a p value ≥ 0.05. Regional statistics were calculated using station-level values including all years aggregated.

Year	Number of year	Number of events					Cumulative precipitation (mm)					Cumulative erosivity (EI_{30} ; $MJ\,mm\,ha^{-1}\,h^{-1}\,yr^{-1}$)						Local minimum		Local maximum	
		Median	25^{th}	75^{th}	Mean	SD	Median	25^{th}	75^{th}	Mean	SD	Median	25^{th}	75^{th}	Mean	SD	Sign test group	Name		Name	
2011	58	21	19	24	21	7	852	715	1055	887	323	3884	2341	5556	4150	2326	a, b, c, d, e, f, i, j	Furudono	161	Nasukougen	11798
2012	57	28	23	35	29	8	916	710	1104	935	324	3303	2531	4049	3618	1903	a, b, c, d, e, f, g, j	Yonezawa	820	Hanazono	9793
2013	58	26	24	29	26	4	936	846	1063	966	153	4213	3319	5221	4458	1793	a, b, c, d, e, f, i	Yanagawa	1846	Daigo	9745
2014	58	30	27	33	30	4	1168	965	1409	1208	311	4446	2808	5731	4665	2087	a, b, c, d, f	Yonezawa	1739	Hanazono	11154
2015	58	30	26	33	30	5	946	742	1180	978	271	3388	2114	4615	3693	2112	a, b, c, e, f, g, j, k	Kitakata	923	Kawauchi	10876
2016	58	28	25	33	29	6	960	824	1104	992	261	3226	2386	4522	3705	1979	a, b, c, d, e, f, g, j, k	Yonezawa	1280	Washikura	12323
2017	58	26	23	29	26	4	926	832	1035	950	204	2718	2090	3586	3048	1287	b, e, f, g, h, j, k	Yanagawa	1100	Ootawara	6954
2018	58	25	22	28	25	5	768	578	918	778	256	1908	1388	3392	2422	1356	g, h, k	Yonezawa	791	Yamada	6305
2019	57	26	25	30	28	5	1068	912	1279	1116	329	6159	3970	8270	6613	3728	a, c, i	Inawashiro	1095	Hanazono	18004
2020	57	26	22	29	26	4	896	797	1036	959	249	3191	2469	4091	3586	1595	a, b, c, d, e, f, g, j, k	Yanagawa	1140	Shinchi	8652
2021	57	31	27	36	31	6	1006	850	1369	1094	338	2595	1689	4879	3386	2101	a, b, e, f, g, j, k	Takahata	654	Hanazono	8041
2022	54	24	22	28	25	4	751	671	889	804	199	2597	2000	3498	3113	1879	e, f, g, h, j, k	Wakamatsu	882	Nihonmatsu	9081
2023	54	26	22	29	26	5	795	650	959	839	254	3081	2219	4860	4016	2843	a, b, c, d, e, f, g, j, k	Konan	619	Hitachi	12419
2024	54	30	25	33	30	6	882	772	1042	930	227	3052	2184	5054	3644	1897	a, b, c, e, f, g, j, k	Yanagawa	1282	Kuroen	10715
Regional summary:		*27*	*23*	*31*	*27*	*6*	*917*	*768*	*1119*	*961*	*291*	*3290*	*2273*	*4947*	*3868*	*2327*	-	-	-	-	-

https://doi.org/10.5194/egusphere-2025-6030
Preprint. Discussion started: 20 January 2026

Table A4. Monthly summary of cumulative rainfall erosivity (EI_{30} or *R*-factor) within a 110-km radius region around FDNPP over the period 2011-2024. Statistics are based on 10-min data from 58 weather stations (data from the Japanese Meteorological Agency). '25th' and '75th' indicate the 25th and 75th quantiles, respectively. 'SD' indicates standard deviation. Sign tests were performed on station-level values and 'Sign test group' indicates statistically undistinguishable groups with a p value ≥ 0.05. Number of months out of the theoretical maximum of 812. Regional statistics were calculated using station-level values with all years aggregated.

Month	Number of month	Number of events					Cumulative precipitation (mm)					Cumulative erosivity (EI_{30}; $MJ\,mm\,ha^{-1}\,h^{-1}\,yr^{-1}$)												
		Median	25th	75th	Mean	SD	Median	25th	75th	Mean	SD	Median	25th	75th	Mean	SD	Sign test group	Local minimum		Local maximum	
																		Name	Year	Name	Year		
January	428	1	1	2	1	1	39	21	62	48	35	22	11	51	76	184	a	Ishikawa	2013	1	Hanazono	2020	1680
February	426	1	1	2	1	1	32	19	48	40	29	19	9	59	72	167	b	Kawauchi	2023	1	Onahama	2021	1592
March	640	2	2	4	3	1	68	42	110	80	51	54	24	131	112	157	c, d	Hibara	2017	1	Hanazono	2018	1266
April	765	2	2	3	3	1	72	46	108	82	51	82	38	171	168	316	c, d, e	Iitate	2019	1	Taira	2013	5402
May	769	2	1	3	2	1	67	43	100	80	56	94	50	212	209	344	d, e, j	Hibara	2020	5	Ootawara	2012	3582
June	773	3	2	4	3	2	87	48	140	104	73	196	75	474	358	459	f, j	Yanagawa	2018	4	Hanazono	2012	4512
July	751	4	2	5	4	2	124	77	182	139	87	552	252	1020	761	736	g, i	Yumoto	2016	8	Shirakawa	2019	5021
August	753	3	2	5	4	2	88	50	171	121	100	400	168	929	751	974	h, i	Natori	2011	7	Washikura	2016	10561
September	787	4	3	5	4	2	140	88	207	159	99	525	234	1142	920	1171	g, h, i	Takahata	2014	8	Hitachi	2023	9286
October	714	3	2	4	3	1	82	42	197	136	134	108	41	515	609	1359	e, f, j	Iwatama	2016	5	Hippo	2019	14894
November	606	2	1	2	2	1	42	24	67	51	35	44	21	91	87	142	k	Washikura	2019	3	Yamada	2021	1463
December	491	1	1	2	2	1	38	22	56	46	32	32	16	62	57	94	k	Inawashiro	2014	1	Taira	2021	894
Regional summary:	*2*	*1*	*4*	*3*	*2*	*71*	*39*	*127*	*97*	*85*	*114*	*37*	*411*	*390*	*768*	-	-	-	-	-	-	-	-

https://doi.org/10.5194/egusphere-2025-6030
Preprint. Discussion started: 20 January 2026

Table A5. Summary of typhoon season (June-October) cumulative precipitation and erosive related cumulative precipitation and erosivity (EI_{30}) and their median and mean relative contributions (in %) to annual total (in brackets) or to cumulated precipitation during the typhoon season (in parentheses) among the 58 weather stations located within the 110-km radius region around FDNPP over the period 2011-2024 (data from Japanese Meteorological Agency). '25^{th}' and '75^{th}' indicate the 25^{th} and 75^{th} quantiles respectively, 'SD' indicates standard deviation, 'Sign test group' indicates Sign test statistically undistinguishable groups (p value ≥ 0.05). Number of station out of the 58 weather stations. Regional medians were statistics from station-level values aggregated across all years.

Year	Number of station	Seasonal cumulative precipitation (mm)							Erosive events																									
									Number of events							Cumulative precipitation (mm)												Cumulative erosivity (EI_{30}; $MJ\,mm\,ha^{-1}\,h^{-1}\,yr^{-1}$)							Local minimum				Local maximum			
		Median		25^{th}	75^{th}	Mean		SD	Sign test group	Median		25^{th}	75^{th}	Mean	SD	Median		25^{th}	75^{th}	Mean		SD	Sign test group	Median		25^{th}	75^{th}	Mean		SD	Sign test group	Name	Prec.	EI_{30}	Name	Prec.	EI_{30}
2011	57	825	[65]	724	888	860	[64]	193	a, c, e, f, h, i	13	[62]	12	16	14	[62]	4	621	(79)	[50]	548	703	646	(78)	[50]	217	a, c, e, f, g, j, k	3444	[90]	2190	4869	3740	[89]	2065	a, c, d, e, f, g, i, j	Furudono	72	80	Nasukougen	1210	10631
2012	57	640	[50]	552	711	648	[48]	164	b, j, l	13	[48]	12	16	14	[48]	4	472	(74)	[37]	402	558	489	(74)	[36]	164	b, e, h, l, n	2308	[71]	1769	2981	2475	[70]	1241	b, e, f, g, h, j, k	Yonezawa	154	593	Nasukougen	944	6486
2013	58	878	[70]	830	964	910	[68]	126	a, c, d, f, i	18	[68]	17	20	18	[69]	2	701	(79)	[55]	636	769	717	(79)	[54]	112	a, c, d, e, f, g, k	3703	[94]	2927	4554	3948	[90]	1576	a, c, d, e, f	Konan	624	1727	Daigo	836	9032
2014	58	950	[60]	801	1035	944	[59]	213	c, d, h	17	[56]	15	19	17	[57]	4	746	(81)	[48]	618	860	758	(79)	[47]	209	c, d, g, j	3722	[86]	2484	4884	3820	[84]	1566	a, c, d, f	Yonezawa	467	1462	Hanazono	1341	8781
2015	58	736	[55]	628	902	768	[55]	189	a, e, h, i, j, k, l	15	[48]	12	16	15	[49]	3	542	(73)	[42]	430	736	577	(73)	[41]	202	a, b, c, e, j, k, l, m, n	2659	[83]	1697	3911	3101	[82]	1979	a, b, c, e, f, g, j, k	Kitakata	297	544	Kawauchi	970	10305
2016	58	806	[64]	729	948	855	[63]	205	a, c, f, h, i	18	[61]	15	20	18	[60]	3	638	(78)	[50]	557	757	675	(78)	[50]	204	a, c, f, g, j, k	2947	[90]	2195	4175	3359	[90]	1890	a, b, c, d, e, f, g, j	Yonezawa	407	1094	Washikura	1579	11725
2017	58	900	[71]	821	992	934	[69]	171	a, c, d, f, i	19	[73]	17	21	19	[72]	4	699	(77)	[54]	623	781	725	(77)	[53]	171	a, c, d, f, g, k	2480	[92]	1907	3283	2775	[91]	1184	a, b, e, f, g, j	Yanagawa	430	938	Ootawara	984	6682
2018	58	640	[56]	561	719	640	[55]	147	b, j, l	14	[56]	12	16	14	[56]	3	468	(72)	[41]	335	542	458	(70)	[39]	155	b, h, l, n	1560	[78]	1016	2756	1876	[77]	1063	b, h, k	Wakamatsu	142	324	Hitachioomiya	584	4241
2019	57	1075	[76]	937	1234	1120	[73]	275	g	19	[71]	17	22	19	[70]	4	868	(80)	[59]	740	997	889	(78)	[58]	266	i	5681	[93]	3765	7377	6157	[92]	3524	a, i	Inawashiro	466	919	Hippo	1357	17244
2020	57	764	[60]	712	896	811	[60]	167	a, d, e, f, h, i, k	17	[68]	15	19	18	[67]	3	564	(74)	[44]	498	682	606	(74)	[44]	166	a, d, e, f, j, k, l, m, n	2255	[78]	1839	3012	2657	[75]	1266	a, b, e, f, g, j, k	Yanagawa	442	887	Shinchi	896	7685
2021	57	820	[57]	702	940	829	[56]	183	a, c, e, f, h, i, j, k	19	[60]	17	23	19	[60]	4	618	(77)	[44]	509	760	628	(75)	[42]	181	a, c, e, f, g, j, k, l, m	2002	[70]	1087	2809	2219	[68]	1311	b, e, h, j, k	Takahata	266	454	Kuroen	856	6101
2022	54	668	[57]	573	758	699	[57]	175	b, e, i, j, k, l	13	[56]	12	16	14	[56]	2	497	(74)	[41]	414	552	515	(73)	[42]	163	b, e, h, j, k, l, m, n	2076	[84]	1524	3086	2674	[83]	1820	b, e, f, g, h, j, k	Wakamatsu	272	611	Nihonmatsu	705	8294
2023	54	700	[64]	604	845	737	[62]	183	e, h, i, j, k, l	16	[61]	14	18	16	[61]	3	527	(75)	[48]	427	677	556	(74)	[46]	177	e, j, k, l, m, n	2675	[87]	1817	4352	3546	[87]	2628	a, b, c, d, e, f, g, j	Konan	263	469	Hitachi	936	11845
2024	54	659	[54]	590	782	702	[53]	169	b, e, j, k, l	16	[56]	14	19	17	[56]	4	464	(72)	[39]	409	604	511	(72)	[39]	153	b, e, h, j, l, m, n	2334	[83]	1594	4117	2939	[80]	1741	a, b, e, f, g, j, k	Yanagawa	304	1042	Kuroen	864	9816
Regional summary:		*793*	*[61]*	*665*	*944*	*820*	*60*	*224*	-	*16*	*[61]*	*14*	*19*	*16*	*[60]*	*4*	*602*	*(76)*	*[46]*	*474*	*749*	*626*	*(75)*	*[46]*	*217*	-	*2698*	*[86]*	*1826*	*4076*	*3236*	*[83]*	*2121*	-	-	-	-	-	-	-

https://doi.org/10.5194/egusphere-2025-6030
Preprint. Discussion started: 20 January 2026

Table A6. Summary of typhoon season (June-October) cumulative precipitation and erosive related cumulative precipitation and erosivity (EI_{30}) relative contribution to monthly (in braces), seasonal (in parentheses), and annual (in brackets) total values among the 58 weather stations located within the 110-km radius region around FDNPP over the period 2011-2024 (data from the Japanese Meteorological Agency). '25^{th}' and '75^{th}' indicate the 25^{th} and 75^{th} quantiles, respectively, 'SD' indicates standard deviation, 'Sign test group' indicates Sign test statistically undistinguishable groups (p value ≥ 0.05). Regional medians were statistics from station-level values aggregated across all years.

Month	Number of month	Seasonal cumulative precipitation (mm)								Erosive events																													
										Number of events							Cumulative precipitation (mm)								Cumulative erosivity (EI_{30} ; $MJ\,mm\,ha^{-1}\,h^{-1}\,yr^{-1}$)								Local minimum						Local maximum				
		Median			25^{th}	75^{th}	Mean			SD	Median			25^{th}	75^{th}	Mean		SD	Median			25^{th}	75^{th}	Mean			SD	Median			25^{th}	75^{th}	Mean			SD	Name	Year	Prec.	Ev. prec.	EI_{30}	Name	Year	Prec.	Ev. prec.	EI_{30}
June	771	125	(16)	[10]	82	180	139	(17)	[10]	74	3	(18)	[10]	2	4	3	(18)	[10]	2	87	{72}	(11)	{7}	141	48	104	{69}	(13)	{8}	73	196	(7)	{6}	75	474	359	(12)	{9}	459	Yanagawa	2018	30	16	4	Hanazono	2012	383	360	4512
July	749	166	(21)	[12]	122	232	186	(23)	[14]	93	4	(22)	[13]	2	5	4	(22)	[13]	2	124	{73}	(15)	{9}	183	78	139	{71}	(17)	{10}	87	552	(21)	{17}	250	1019	761	(26)	{21}	737	Yumoto	2016	42	16	8	Shirakawa	2019	340	284	5021
August	752	138	(18)	[11]	98	219	166	(20)	[12]	101	3	(20)	[12]	2	5	4	(20)	[12]	2	88	{68}	(11)	{7}	171	50	121	{66}	(15)	{9}	100	398	(17)	{13}	168	929	751	(25)	{20}	974	Natori	2011	32	13	7	Washikura	2016	932	902	10561
September	785	170	(23)	{13}	124	238	192	(24)	[14]	97	4	(22)	{14}	3	5	4	(22)	{14}	2	140	{81}	(18)	{11}	206	88	159	{78}	(20)	{12}	99	525	(22)	{18}	230	1140	915	(28)	{23}	1161	Takahata	2014	32	16	8	Hitachi	2023	436	432	9286
October	709	118	(16)	{8}	76	225	168	(19)	{12}	136	3	(16)	{10}	2	4	3	(16)	{10}	1	82	{76}	(11)	{6}	198	41	136	{72}	(15)	{10}	134	107	(4)	{3}	41	515	609	(14)	{12}	1362	Iwatama	2016	34	13	5	Hippo	2019	902	856	14894
Regional summary:		*146*	*(19)*	*[11]*	*98*	*217*	*170*	*(21)*	*[12]*	*103*	*3*	*(20)*	*[12]*	*2*	*5*	*4*	*(20)*	*[12]*	*2*	*106*	*{75}*	*(14)*	*{8}*	*179*	*58*	*132*	*{71}*	*(16)*	*{10}*	*102*	*354*	*(14)*	*[11]*	*118*	*830*	*680*	*(21)*	*[17]*	*1003*	-	-	-	-	-	-	-	-	-	-

https://doi.org/10.5194/egusphere-2025-6030
Preprint. Discussion started: 20 January 2026

Table A7. Summary of median erosivity (EI_{30}) of the typhoon season (June-October) erosive events ranked according to their intensity along with their relative contribution to seasonal (in parentheses) and annual (in brackets) total values among the 58 weather stations located within the 110-km radius region around FDNPP over the period 2011-2024 (data from Japanese Meteorological Agency). Regional statistics were calculated using station-level values all years aggregated.

Year	Median num. of events	Ranked typhoon season erosive events erosivity (EI_{30}; $MJ\,mm\,ha^{-1}\,h^{-1}\,yr^{-1}$)																		
		Rank: 1	2	3	4	5	6	7	8	9	10	11	12	13	14	15	16	17	18	19
2011	13	1643 (48) [44]	510 (17) [14]	269 (9) [7]	185 (6) [5]	106 (4) [4]	87 (3) [2]	70 (2) [2]	55 (2) [2]	52 (2) [1]	40 (1) [1]	29 (1) [1]	26 (1) [1]	26 (1) [1]						
2012	13	733 (35) [25]	411 (20) [13]	254 (12) [8]	194 (9) [6]	142 (7) [4]	100 (4) [3]	74 (3) [2]	51 (2) [2]	38 (2) [1]	30 (1) [1]	23 (1) [1]	17 (1) [0]	15 (1) [0]						
2013	18	978 (29) [27]	537 (16) [15]	413 (11) [10]	294 (8) [7]	217 (6) [6]	153 (5) [4]	130 (4) [3]	113 (3) [3]	95 (2) [2]	73 (2) [2]	59 (2) [2]	48 (2) [1]	43 (1) [1]	32 (1) [1]	28 (1) [1]	24 (1) [1]	22 (1) [0]	18 (0) [0]	
2014	17	1088 (28) [24]	558 (17) [14]	432 (12) [10]	299 (9) [7]	206 (7) [6]	152 (5) [4]	130 (4) [4]	108 (3) [2]	83 (2) [2]	70 (2) [2]	58 (2) [1]	53 (1) [1]	39 (1) [1]	30 (1) [1]	25 (1) [0]	22 (1) [0]	17 (0) [0]		
2015	15	1350 (46) [38]	418 (16) [13]	212 (9) [7]	122 (6) [4]	94 (4) [3]	72 (3) [2]	50 (2) [2]	40 (2) [1]	34 (2) [1]	27 (1) [1]	22 (1) [1]	16 (1) [1]	16 (0) [0]	14 (0) [0]	13 (0) [0]				
2016	18	1044 (34) [30]	544 (19) [17]	322 (12) [11]	220 (8) [7]	144 (5) [5]	115 (4) [4]	84 (3) [3]	66 (2) [2]	55 (2) [2]	45 (2) [1]	38 (1) [1]	35 (1) [1]	26 (1) [1]	22 (1) [1]	20 (1) [1]	23 (1) [1]	20 (0) [0]	18 (0) [0]	
2017	19	820 (31) [29]	380 (17) [16]	240 (11) [10]	172 (8) [7]	134 (6) [5]	111 (4) [4]	88 (4) [4]	80 (3) [3]	62 (2) [2]	54 (2) [2]	44 (2) [2]	36 (1) [1]	28 (1) [1]	26 (1) [1]	20 (1) [1]	17 (1) [1]	13 (1) [0]	11 (0) [0]	13 (1) [0]
2018	14	519 (32) [24]	263 (19) [14]	190 (12) [9]	141 (9) [7]	94 (7) [5]	78 (5) [4]	62 (4) [3]	46 (3) [2]	33 (2) [2]	27 (2) [1]	21 (1) [1]	18 (1) [1]	17 (1) [1]	14 (1) [1]					
2019	19	2968 (48) [44]	981 (16) [15]	402 (6) [7]	259 (5) [5]	183 (4) [4]	148 (3) [3]	109 (2) [2]	92 (2) [2]	79 (2) [2]	64 (1) [1]	51 (1) [1]	41 (1) [1]	32 (1) [1]	28 (1) [0]	25 (0) [0]	20 (0) [0]	17 (0) [0]	16 (0) [0]	15 (0) [0]
2020	17	757 (34) [25]	442 (18) [13]	246 (11) [8]	177 (9) [6]	133 (6) [4]	108 (5) [3]	81 (3) [2]	66 (3) [2]	52 (2) [2]	40 (2) [1]	32 (2) [1]	24 (1) [1]	19 (1) [1]	16 (1) [1]	14 (1) [0]	13 (1) [0]	11 (0) [0]		
2021	19	461 (26) [17]	297 (16) [11]	179 (10) [7]	152 (8) [5]	111 (6) [4]	102 (5) [3]	86 (4) [3]	74 (4) [2]	71 (3) [2]	63 (3) [2]	55 (2) [2]	49 (2) [1]	39 (2) [1]	35 (2) [1]	29 (1) [1]	25 (1) [1]	21 (1) [0]	16 (1) [0]	16 (1) [0]
2022	13	632 (33) [27]	388 (18) [15]	262 (12) [10]	162 (8) [6]	114 (6) [5]	96 (5) [4]	76 (4) [3]	62 (3) [2]	46 (2) [2]	36 (2) [1]	28 (2) [1]	22 (1) [1]	18 (1) [1]						
2023	16	926 (31) [27]	399 (17) [14]	255 (12) [10]	192 (8) [7]	140 (6) [5]	110 (4) [4]	85 (4) [3]	72 (3) [2]	50 (2) [2]	36 (2) [1]	32 (1) [1]	28 (1) [1]	21 (1) [1]	18 (1) [1]	17 (1) [0]	18 (0) [0]			
2024	16	845 (34) [27]	443 (18) [15]	283 (12) [9]	172 (7) [6]	124 (6) [4]	100 (4) [3]	74 (4) [3]	60 (3) [2]	52 (2) [2]	41 (2) [1]	37 (1) [1]	32 (1) [1]	31 (1) [1]	27 (1) [1]	24 (1) [1]	20 (1) [0]	18 (0) [0]		
Regional summary:	*91.2*	*(35)* [28]	*443*	*(17)* [14]	*278*	*(11)* [9]	*188*	*(8)* [6]	*141*	*(6)* [4]	*108*	*(4)* [3]	*84*	*(3)* [2]	*68*	*(3)* [2]	*55*	*(2)* [2]	*45*	*(2)* [1]	*35*	*(1)* [1]	*28*	*(1)* [1]	*21*	*(1)* [1]	*14*	*(0)* [0]	*10*	*(0)* [0]	*0*	*(0)* [0]	*0*	*(0)* [0]

https://doi.org/10.5194/egusphere-2025-6030
Preprint. Discussion started: 20 January 2026

Table A8. Annual summary of median cumulative precipitation of the typhoon season (June-October) erosive events, ranked by their erosivity intensity (EI_{30}). Relative contributions to erosive events (in braces), seasonal (in parentheses) and annual (in brackets) total values are shown. Statistics are based on data from 58 weather stations within a 110 km radius region around the FDNPP over the period 2011-2024 (data from theJapanese Meteorological Agency). Regional medians were calculated from station-level values aggregated across all years.

Year	Median cum. no. of events	Rank-1	2	3	4	5	6	7	8	Ranks of typhoon season erosive events (cumulative precipitation (mm)) 9	10	11	12	13	14	15	16	17	18	19
2011	13	226 {33} (15)	62 {10} (10) {5}	50 {8} (7) {4}	35 {6} (6) {3}	30 {5} (4) {2}	26 {4} (4) {2}	41 {6} (5) {3}	24 {4} (4) {2}	24 {4} (4) {2}	16 {3} (3) {1}	20 {3} (3) {1}	19 {3} (3) {2}	20 {3} (2) {1}							
2012	13	80 {19} (18) {7}	56 {12} (12) {4}	44 {10} (9) {4}	39 {8} (8) {3}	22 {6} (6) {2}	34 {5} (5) {2}	26 {6} (6) {2}	21 {5} (5) {2}	20 {4} (4) {2}	20 {4} (4) {1}	16 {4} (4) {1}	18 {4} (4) {1}								
2013	18	80 {14} (13) {8}	75 {11} (11) {6}	56 {9} (9) {5}	54 {8} (8) {4}	43 {6} (6) {3}	38 {5} (5) {3}	32 {5} (5) {3}	33 {5} (5) {2}	28 {4} (4) {2}	26 {4} (4) {2}	27 {4} (4) {2}	21 {3} (3) {2}	19 {3} (3) {2}	20 {3} (3) {2}		18 {2} (2) {1}	18 {2} (2) {1}	17 {2} (2) {1}		
2014	17	111 {16} (15) {7}	78 {12} (11) {5}	76 {10} (10) {5}	57 {7} (7) {4}	54 {7} (7) {3}	42 {6} (6) {3}	34 {5} (5) {2}	34 {5} (5) {2}	32 {4} (4) {2}	30 {4} (4) {2}	25 {4} (4) {2}	24 {4} (3) {2}	19 {3} (3) {1}	21 {3} (3) {1}	21 {3} (3) {1}	20 {3} (3) {1}	16 {2} (2) {1}			
2015	15	131 {25} {24} {10}	60 {11} (11) {4}	40 {8} (8) {3}	34 {7} (7) {3}	30 {6} (6) {2}	27 {6} (6) {2}	26 {5} (5) {2}	22 {4} (4) {2}	24 {5} (5) {2}	19 {4} (4) {1}	20 {4} (4) {1}	18 {4} (4) {1}	18 {3} (3) {1}	16 {3} (3) {1}	17 {3} (3) {1}	18 {3} (3) {1}	16 {2} (2) {1}			
2016	18	91 {16} (15) {7}	67 {11} (11) {6}	63 {10} (10) {5}	46 {7} (7) {4}	35 {6} (6) {3}	40 {8} (8) {3}	36 {6} (6) {3}	27 {5} (5) {2}	30 {5} (5) {2}	25 {4} (4) {2}	25 {4} (4) {2}	21 {4} (3) {2}	20 {3} (3) {2}	21 {3} (3) {2}	21 {3} (3) {2}	20 {3} (3) {2}	18 {3} (3) {1}	16 {2} (2) {1}		
2017	19	136 {23} {11}	77 {14} {6}	54 {10} {5}	44 {7} {4}	39 {6} {3}	35 {5} {2}	27 {4} {2}	30 {4} {2}	29 {5} {2}	21 {4} {2}	23 {4} {2}	21 {4} {2}	20 {3} {2}	19 {3} {2}	20 {3} {2}	17 {2} {2}	18 {3} {2}	17 {2} {2}	18 {2} {2}	{2} {1}
2018	14	55 {15} {14} {9}	54 {13} {12} {4}	44 {9} {9} {4}	29 {8} {8} {3}	29 {7} {7} {3}	25 {8} {7} {2}	22 {6} {6} {2}	23 {6} {6} {2}	20 {5} {5} {2}	19 {5} {5} {2}	17 {4} {4} {2}	18 {4} {4} {2}	18 {4} {4} {2}	16 {3} {3} {1}	16 {3} {3} {1}	16 {3} {3} {1}	16 {3} {3} {1}	17 {2} {2} {1}	19 {2} {3} {1}
2019	19	241 {29} {16}	97 {11} {11} {6}	59 {7} {7} {4}	42 {6} {5} {3}	34 {4} {4} {2}	33 {5} {4} {2}	31 {4} {4} {2}	30 {4} {4} {2}	27 {3} {3} {2}	24 {3} {3} {2}	22 {3} {3} {2}	22 {3} {3} {2}	21 {3} {2} {1}	20 {2} {2} {1}	16 {2} {2} {1}	18 {2} {2} {1}	16 {2} {2} {1}	17 {2} {2} {1}	19 {2} {3} {1}	
2020	17	82 {15} {15} {6}	58 {11} {10} {4}	42 {8} {7} {3}	37 {8} {7} {3}	33 {6} {6} {2}	27 {5} {5} {2}	26 {5} {5} {2}	26 {4} {4} {2}	24 {4} {4} {2}	24 {5} {4} {2}	19 {4} {4} {2}	20 {4} {4} {2}	18 {3} {3} {1}	16 {3} {3} {1}	16 {3} {3} {1}	16 {3} {3} {1}	16 {3} {3} {1}			
2021	19	49 {9} {9} {4}	46 {8} {8} {3}	44 {7} {7} {3}	34 {6} {6} {2}	31 {5} {4} {2}	31 {6} {5} {2}	32 {6} {6} {2}	36 {7} {7} {3}	31 {5} {5} {2}	28 {5} {5} {2}	24 {5} {5} {2}	25 {4} {4} {2}	22 {4} {4} {2}	23 {4} {4} {2}	23 {4} {4} {1}	20 {3} {3} {1}	18 {3} {3} {1}	18 {3} {3} {1}	18 {3} {3} {1}	
2022	13	77 {16} {16} {7}	59 {12} {12} {5}	52 {10} {10} {4}	36 {8} {7} {3}	30 {6} {6} {2}	28 {6} {6} {2}	34 {5} {5} {2}	23 {5} {5} {2}	22 {4} {4} {2}	19 {4} {4} {2}	24 {5} {5} {2}	18 {4} {4} {2}	18 {4} {4} {2}	18 {4} {4} {1}						
2023	16	72 {16} {15} {7}	58 {11} {11} {5}	43 {8} {8} {3}	34 {7} {7} {3}	36 {6} {6} {3}	26 {5} {5} {2}	30 {6} {6} {2}	24 {5} {5} {2}	28 {6} {6} {2}	21 {4} {4} {2}	21 {4} {4} {2}	21 {5} {4} {2}	22 {4} {4} {2}	20 {4} {4} {2}	20 {4} {3} {2}					
2024	16	70 {15} {15} {6}	48 {10} {9} {4}	44 {8} {8} {3}	34 {7} {7} {3}	30 {6} {6} {2}	26 {5} {5} {2}	21 {5} {5} {2}	21 {5} {5} {2}	20 {4} {4} {2}	20 {5} {4} {2}	18 {4} {4} {2}	18 {4} {4} {2}	18 {4} {4} {2}	20 {4} {4} {2}	18 {4} {4} {2}					
Regional summary:	94 {17} {16} {7}	63 {12} {12} {5}	49 {8} {8} {4}	39 {7} {7} {3}	33 {6} {6} {2}	30 {5} {5} {2}	28 {5} {5} {2}	26 {5} {5} {2}	24 {4} {4} {2}	22 {4} {4} {2}	20 {4} {4} {2}	20 {4} {3} {2}	18 {3} {3} {2}	18 {3} {3} {1}	17 {3} {3} {1}	16 {3} {3} {1}	16 {3} {3} {1}	16 {3} {3} {1}	16 {3} {3} {1}	17 {2} {2} {1}	18 {3} {3} {1}

https://doi.org/10.5194/egusphere-2025-6030
Preprint. Discussion started: 20 January 2026

Table A9. Annual summary of the three most erosive events that occurred during the typhoon season (June-October) within a 110 km radius region around the FDNPP over the period 2011-2024. Relative contributions to erosive events (in braces), seasonal (in parentheses) and annual (in brackets) total values are shown. Statistics are based on data from 58 weather stations (data from the Japanese Meteorological Agency). Regional medians were calculated from station-level values aggregated across all years. Sign test were performed on station-level values.

		Three leading typhoon season erosive event																											
		Cumulative precipitation (mm)										Cumulative erosivity (EI_{30} ; $MJ\,mm\,ha^{-1}\,h^{-1}\,yr^{-1}$)										Local minimum				Local maximum			
Year	Number of station	Median			25th	75th	Mean		SD	Sign test group	Median			25th	75th	Mean		SD	Sign test group	Name	Prec.	EI_{30}	Name	Prec.	EI_{30}		
2011	53	336	{55}	(53)	[26]	308	396	347	{55}	(52)	[26]	70	a	2788	(77)	[67]	1779	3673	2897	(76)	[67]	1316	a, c, d, g, k	Hibara	302	966	Nasukougen	534	6885
2012	57	184	{45}	(42)	[14]	156	238	202	{45}	(43)	[15]	70	b, e, f, h, i, j, k	1465	(68)	[48]	1193	2058	1683	(69)	[48]	903	b, c, d, e, h, i, j, k	Kaminoyamasakayama	61	401	Hanazono	392	5391
2013	57	234	{35}	(35)	[19]	207	278	243	{35}	(34)	[18]	50	c, d, e, f, g, i, j, k	2110	(62)	[56]	1453	3004	2438	(60)	[54]	1273	a, b, c, d, e, h, j, k	Kitakata	126	598	Ishikawa	342	6232
2014	58	269	{39}	(38)	[17]	232	323	280	{39}	(38)	[18]	72	c, d, e, f, g, i	2088	(60)	[49]	1598	3066	2311	(62)	[51]	1019	a, b, c, d, j, k	Nihonmatsu	219	844	Shinchi	424	5250
2015	58	252	{48}	(46)	[19]	192	343	281	{49}	(48)	[20]	137	b, c, d, e, f, g, i, k	2118	(79)	[65]	1367	2938	2495	(77)	[64]	1881	a, b, c, d, e, h, j, k	Kitakata	104	295	Kawauchi	664	9593
2016	58	213	{36}	(35)	[17]	192	280	242	{37}	(36)	[18]	80	b, c, d, e, f, g, i, j	2018	(64)	[58]	1232	2643	2231	(66)	[59]	1323	a, b, c, d, e, h, j, k	Hibara	176	537	Washikura	628	8355
2017	58	262	{39}	(38)	[21]	215	337	278	{40}	(38)	[21]	87	c, d, e, f, g	1502	(63)	[58]	1038	2278	1732	(61)	[56]	861	b, c, e, f, h, j, k	Yanagawa	179	424	Ootawara	322	4123
2018	58	158	{38}	(36)	[14]	117	196	168	{38}	(37)	[14]	70	b, h, i, j, k	1066	(65)	[50]	678	1822	1226	(65)	[50]	730	e, f, h, i, j	Wakamatsu	63	231	Furudono	270	2836
2019	57	410	{48}	(47)	[27]	330	518	426	{49}	(48)	[28]	148	a	4468	(76)	[68]	2541	6009	4753	(75)	[69]	3003	a, g	Hibara	202	551	Hippo	860	15761
2020	57	196	{36}	(36)	[16]	156	258	221	{38}	(37)	[16]	88	b, c, d, e, f, h, i, j, k	1421	(66)	[50]	1058	2093	1758	(65)	[48]	1095	b, c, e, f, h, i, j, k	Hitachi	126	538	Shinchi	563	7189
2021	57	164	{28}	(27)	[11]	126	208	170	{29}	(28)	[11]	60	b, h, i, j, k	976	(53)	[36]	622	1606	1204	(55)	[38]	807	b, f, h, i, j, k	Yanagawa	134	322	Kuroen	224	4321
2022	54	199	{42}	(41)	[17]	162	264	222	{44}	(42)	[18]	100	b, c, f, h, i, j, k	1336	(66)	[51]	1005	2136	1878	(67)	[56]	1551	b, c, d, e, f, h, i, j, k	Wakamatsu	57	305	Nihonmatsu	310	6876
2023	54	190	{35}	(34)	[15]	126	234	207	{37}	(36)	[17]	109	b, c, e, h, i, j, k	1830	(68)	[57]	1046	3089	2485	(66)	[58]	2204	a, b, c, d, e, h, i, j, k	Konan	46	261	Hitachi	550	10134
2024	54	159	{36}	(35)	[13]	134	209	174	{36}	(35)	[13]	55	b, h, i, j, k	1442	(65)	[51]	1114	2290	1873	(65)	[52]	1116	a, b, c, d, e, h, i, j, k	Tomioka	89	542	Kuroen	287	5260
Regional summary:		*224*	*{40}*	*(38)*	*[17]*	*170*	*305*	*247*	*41*	*(39)*	*[18]*	*113*	-	*1753*	*(67)*	*[55]*	*1106*	*2744*	*2208*	*(66)*	*[55]*	*1704*	-	-	-	-	-	-	-	-

https://doi.org/10.5194/egusphere-2025-6030
Preprint. Discussion started: 20 January 2026

Table A10. Annual summary of the most erosive event that occurred during the typhoon season (June-October) within a 110 km radius region around the FDNPP over the period 2011-2024. Relative contributions to erosive events (in braces), seasonal (in parentheses) and annual (in brackets) total values are shown. Statistics are based on data from 58 weather stations (data from the Japanese Meteorological Agency). Regional medians were calculated from station-level values aggregated across all years. Sign test were performed on station-level values.

		First leading typhoon season erosive event																											
		Cumulative precipitation (mm)												Cumulative erosivity (EI_{30} ; $MJ\,mm\,ha^{-1}\,h^{-1}\,yr^{-1}$)										Local minimum			Local maximum		
Year	Number of station	Median				25th	75th	Mean				SD	Sign test group	Median			25th	75th	Mean			SD	Sign test group	Name	Prec.	EI_{30}	Name	Prec.	EI_{30}
2011	53	226	{33}	(32)	[15]	158	258	209	{33}	(32)	[16]	71	a	1643	(48)	[44]	1149	2562	1929	(50)	[44]	1098	a, d, g, i	Hibara	65	417	Natori	336	5580
2012	57	80	{19}	(18)	[7]	46	122	91	{19}	(18)	[6]	55	b, c, d, f, h, i, j, k, l, m	733	(35)	[25]	522	1098	928	(37)	[25]	707	b, c, d, e, f, i	Kaminoyamasakayama	19	152	Hanazono	285	4413
2013	57	89	{14}	(13)	[8]	68	121	95	{13}	(13)	[7]	36	b, c, d, e, f, g, i, j, k, l, m	978	(29)	[27]	643	1671	1311	(32)	[29]	854	b, c, d, e, i	Kitakata	56	213	Ootawara	122	3754
2014	58	111	{16}	(15)	[7]	91	151	117	{17}	(16)	[7]	43	b, c, d, e, f, g, i, k, l	1088	(28)	[24]	744	1442	1198	(32)	[27]	670	b, c, d, e, i	Iitate	96	313	Shinchi	168	3537
2015	58	131	{25}	(24)	[10]	100	166	158	{27}	(26)	[11]	114	c, d, e, f, g, l	1350	(46)	[38]	761	1896	1617	(49)	[40]	1449	a, b, c, d, e, i	Kitakata	60	141	Hippo	572	8941
2016	58	91	{16}	(15)	[7]	74	122	99	{15}	(15)	[7]	34	b, c, d, e, f, g, i, k, l, m	1044	(34)	[30]	609	1569	1166	(35)	[31]	663	b, c, d, e, i	Hibara	65	274	Washikura	120	3238
2017	58	136	{22}	(20)	[11]	63	218	141	{20}	(19)	[10]	83	c, d, e, f, g, i, k, l, m	820	(31)	[29]	466	1347	980	(34)	[31]	632	b, c, d, e, f, h, i	Yanagawa	25	149	Souma	240	2736
2018	58	55	{15}	(14)	[5]	41	82	66	{15}	(14)	[6]	40	b, h, j, k, l, m	519	(32)	[24]	310	848	629	(33)	[26]	422	b, e, f, h, i	Hibara	34	100	Kuroen	66	1766
2019	57	241	{29}	(29)	[16]	193	302	250	{29}	(28)	[16]	107	a	2968	(48)	[44]	1545	3926	3135	(49)	[46]	2297	a, g	Hibara	66	207	Hippo	594	13690
2020	57	82	{15}	(15)	[6]	58	127	97	{17}	(16)	[7]	53	b, c, d, f, g, i, k, l, m	757	(34)	[25]	554	1254	997	(35)	[27]	873	b, c, d, e, f, h, i	Hitachi	47	201	Shinchi	264	5968
2021	57	49	{9}	(9)	[4]	35	72	64	{10}	(10)	[4]	45	b, c, h, j, k, l, m	461	(26)	[17]	349	810	598	(28)	[19]	428	e, f, h, i	Shiroishi	55	121	Ootawara	82	2174
2022	54	77	{16}	(16)	[7]	48	136	101	{19}	(19)	[8]	71	b, c, d, f, g, h, i, j, k, l, m	632	(33)	[27]	439	1192	1099	(37)	[31]	1148	b, c, d, e, f, h, i	Wakamatsu	21	133	Kitakata	276	4660
2023	54	72	{16}	(15)	[7]	50	94	88	{16}	(15)	[7]	56	b, c, d, e, f, g, h, i, j, k, l, m	926	(31)	[27]	444	1660	1464	(36)	[32]	1617	a, b, c, d, e, f, h, i	Konan	16	96	Hitachi	282	7927
2024	54	70	{15}	(15)	[6]	54	96	76	{16}	(15)	[6]	34	b, c, f, g, h, i, j, k, l, m	845	(34)	[27]	523	1151	1014	(35)	[28]	695	b, c, d, e, f, h, i	Tomioka	26	246	Kitakata	108	3278
Regional summary:		*94*	*{17}*	*(16)*	[7]	*58*	*156*	*118*	*19*	*(18)*	[8]	*83*	-	*912*	*(35)*	[28]	*518*	*1602*	*1287*	*(37)*	[31]	*1243*	-	-	-	-	-	-	-

https://doi.org/10.5194/egusphere-2025-6030
Preprint. Discussion started: 20 January 2026

Author contributions. **Thomas Chalaux-Clergue**: Conceptualization, Software, Formal analysis, Data Curation, Writing - Original Draft, Visualization; **Pierre-Alexis Chaboche**: Conceptualization, Writing - Review & Editing; **Yoshifumi Wakiyama**: Writing - Review & Editing; **Olivier Evrard**: Conceptualization, Writing - Review & Editing, Resources, Funding acquisition.

Competing interests. The authors declare that they have no conflict of interest.

Acknowledgements.

Financial support.

The support of CEA (Commissariat à l'Energie Atomique et aux Energies Alternatives, France), CNRS (Centre National de la Recherche Scientifique, France) and JSPS (Japan Society for the Promotion of Science; PE22708) through the funding of PhD fellowships (Thomas Chalaux-Clergue) and collaboration projects (grant no. PRC CNRS JSPS 2019-2020, no. 10; CNRS International Research Laboration - IRL 2039 Mitate Labb) is also recognised.

https://doi.org/10.5194/egusphere-2025-6030
Preprint. Discussion started: 20 January 2026

References

Auerswald, K., Fischer, F. K., Winterrath, T., and Brandhuber, R.: Rain erosivity map for Germany derived from contiguous radar rain data, Hydrology and Earth System Sciences, 23, 1819–1832, https://doi.org/10.5194/hess-23-1819-2019, 2019.

Beck, H. E., Zimmermann, N. E., McVicar, T. R., Vergopolan, N., Berg, A., and Wood, E. F.: Present and future Köppen-Geiger climate classification maps at 1-km resolution, Scientific Data, 5, 180 214, https://doi.org/10.1038/sdata.2018.214, 2018.

Brown, L. and Foster, G. R.: storm Erosivity Using Idealized Intensity Distributions, Transactions of the ASAE, 30, 0379–0386, https://doi.org/10.13031/2013.31957, 1987.

Chalaux-Clergue, T.: RainErosivity: Customisable Tools to Calculate Precipitation Event Rainfall Erosivity Index, https://doi.org/10.5281/ZENODO.16088184, language: en, 2025.

Chalaux-Clergue, T., Bizeul, R., Batista, P. V. G., Martínez-Carreras, N., Laceby, J. P., and Evrard, O.: Sensitivity of source sediment fingerprinting to tracer selection methods, SOIL, 10, 109–138, https://doi.org/10.5194/soil-10-109-2024, 2024a.

Chalaux-Clergue, T., Foucher, A., Chaboche, P.-A., Hayashi, S., Tsuji, H., Wakiyama, Y., Huon, S., Vandromme, R., Cerdan, O., Nakao, A., and Evrard, O.: Impacts of farmland decontamination on 137Cs transfers in rivers after Fukushima nuclear accident: Evidence from a retrospective sediment core study, Science of The Total Environment, 947, 174 546, https://doi.org/10.1016/j.scitotenv.2024.174546, 2024b.

Chalaux-Clergue, T., Chaboche, P.-A., Wakiyama, Y., and Evrard, O.: Precipitation and rainfall erosivity datasets for Northeastern Japan over 2011-2024: 10-minute precipitation records, rainfall event characteristics, and processed summary tables (year, month, typhoon season, single most and three most erosive events) from 58 JMA weather stations located within a 110-km radius around Fukushima Dai-ichi Nuclear Power Plant., https://doi.org/10.5281/zenodo.17573969, 2025.

Chartin, C., Evrard, O., Onda, Y., Patin, J., Lefèvre, I., Ottlé, C., Ayrault, S., Lepage, H., and Bonté, P.: Tracking the early dispersion of contaminated sediment along rivers draining the Fukushima radioactive pollution plume, Anthropocene, 1, 23–34, https://doi.org/10.1016/j.ancene.2013.07.001, 2013.

Chartin, C., Evrard, O., Laceby, J. P., Onda, Y., Ottlé, C., Lefèvre, I., and Cerdan, O.: The impact of typhoons on sediment connectivity: lessons learnt from contaminated coastal catchments of the Fukushima Prefecture (Japan): Typhoon Impact on Sediment Connectivity - Fukushima, Japan, Earth Surface Processes and Landforms, 42, 306–317, https://doi.org/10.1002/esp.4056, 2017.

Cremonini, R., Voormansik, T., Post, P., and Moisseev, D.: Estimation of extreme precipitation events in Estonia and Italy using dual-polarization weather radar quantitative precipitation estimations, Atmospheric Measurement Techniques, 16, 2943–2956, https://doi.org/10.5194/amt-16-2943-2023, 2023.

Diacre, A., Chalaux-Clergue, T., Burban, S., Gauthier, C., Hubert, A., Humbert, A.-C., Lefevre, I., Fauré, A.-L., Pointurier, F., and Evrard, O.: Temporal evolution of plutonium concentrations and isotopic ratios in the Ukedo - Takase Rivers draining the Difficult-To-Return zone in Fukushima, Japan (2013–2020), Environmental Pollution, 319, 120 963, https://doi.org/10.1016/j.envpol.2022.120963, 2023.

Duan, W., He, B., Takara, K., Luo, P., Hu, M., Alias, N. E., and Nover, D.: Changes of precipitation amounts and extremes over Japan between 1901 and 2012 and their connection to climate indices, Climate Dynamics, 45, 2273–2292, https://doi.org/10.1007/s00382-015-2778-8, 2015.

Evrard, O., Chartin, C., Onda, Y., Lepage, H., Cerdan, O., Lefèvre, I., and Ayrault, S.: Renewed soil erosion and remobilisation of radioactive sediment in Fukushima coastal rivers after the 2013 typhoons, Scientific Reports, 4, 4574, https://doi.org/10.1038/srep04574, number: 1 Publisher: Nature Publishing Group, 2014.

https://doi.org/10.5194/egusphere-2025-6030
Preprint. Discussion started: 20 January 2026

Evrard, O., Laceby, J. P., Lepage, H., Onda, Y., Cerdan, O., and Ayrault, S.: Radiocesium transfer from hillslopes to the Pacific Ocean after the Fukushima Nuclear Power Plant accident: A review, Journal of Environmental Radioactivity, 148, 92–110, https://doi.org/10.1016/j.jenvrad.2015.06.018, 2015.

Evrard, O., Durand, R., Nakao, A., Laceby, P. J., Lefèvre, I., Wakiyama, Y., Hayashi, S., Asanuma-Brice, C., and Cerdan, O.: Impact of the 2019 typhoons on sediment source contributions and radiocesium concentrations in rivers draining the Fukushima radioactive plume, Japan, Comptes Rendus. Géoscience, 352, 199–211, https://doi.org/10.5802/crgeos.42, 2020.

Evrard, O., Chalaux-Clergue, T., Chaboche, P.-A., Wakiyama, Y., and Thiry, Y.: Research and management challenges following soil and landscape decontamination at the onset of the reopening of the Difficult-To-Return Zone, Fukushima (Japan), SOIL, 9, 479–497, https://doi.org/10.5194/soil-9-479-2023, 2023.

Fairman, J. G., Schultz, D. M., Kirshbaum, D. J., Gray, S. L., and Barrett, A. I.: A radar-based rainfall climatology of Great Britain and Ireland, Weather, 70, 153–158, https://doi.org/10.1002/wea.2486, 2015.

Golosov, V., Konoplev, A., Wakiyama, Y., Ivanov, M., and Komissarov, M.: Erosion and Redeposition of Sediments and Sediment-Associated Radiocesium on River Floodplains (the Niida River Basin and the Abukuma River as an Example), in: Behavior of Radionuclides in the Environment III, edited by Nanba, K., Konoplev, A., and Wada, T., pp. 97–133, Springer Singapore, Singapore, ISBN 978-981-16-6798-5 978-981-16-6799-2, https://doi.org/10.1007/978-981-16-6799-2_7, 2022.

Hatsuzuka, D. and Sato, T.: Future Changes in Monthly Extreme Precipitation in Japan Using Large-Ensemble Regional Climate Simulations, Journal of Hydrometeorology, 20, 563–574, https://doi.org/10.1175/JHM-D-18-0095.1, 2019.

Hazet, P., Foucher, A., Evrard, O., and Quesada, B.: Impact of rainfall variability on sedimentary and hydropower dynamics in a dam reservoir of southern France, https://doi.org/10.5194/egusphere-2025-2127, 2025.

Huon, S., Hayashi, S., Laceby, J. P., Tsuji, H., Onda, Y., and Evrard, O.: Source dynamics of radiocesium-contaminated particulate matter deposited in an agricultural water reservoir after the Fukushima nuclear accident, Science of The Total Environment, 612, 1079–1090, https://doi.org/10.1016/j.scitotenv.2017.07.205, 2018.

Ikenoue, T., Shimadera, H., and Kondo, A.: Impact of soil erosion potential uncertainties on numerical simulations of the environmental fate of radiocesium in the Abukuma River basin, Journal of Environmental Radioactivity, 225, 106 452, https://doi.org/10.1016/j.jenvrad.2020.106452, 2020.

Iwagami, S., Onda, Y., Tsujimura, M., and Abe, Y.: Contribution of radioactive 137Cs discharge by suspended sediment, coarse organic matter, and dissolved fraction from a headwater catchment in Fukushima after the Fukushima Dai-ichi Nuclear Power Plant accident, Journal of Environmental Radioactivity, 166, 466–474, https://doi.org/10.1016/j.jenvrad.2016.07.025, 2017.

JMA: Historical weather data of Japan, https://www.data.jma.go.jp/stats/etrn/index.php, 2024.

JMA: Weather events causing disasters (1989–present) ()), https://www.data.jma.go.jp/stats/data/bosai/report/index_1989.html, 2025.

Kato, H., Onda, Y., and Teramage, M.: Depth distribution of 137Cs, 134Cs, and 131I in soil profile after Fukushima Dai-ichi Nuclear Power Plant Accident, Journal of Environmental Radioactivity, 111, 59–64, https://doi.org/10.1016/j.jenvrad.2011.10.003, 2012.

Kato, H., Onda, Y., Gao, X., Sanada, Y., and Saito, K.: Reconstruction of a Fukushima accident-derived radiocesium fallout map for environmental transfer studies, Journal of Environmental Radioactivity, 210, 105 996, https://doi.org/10.1016/j.jenvrad.2019.105996, 2019.

Kawase, H., Nosaka, M., Watanabe, S. I., Yamamoto, K., Shimura, T., Naka, Y., Wu, Y., Okachi, H., Hoshino, T., Ito, R., Sugimoto, S., Suzuki, C., Fukui, S., Takemi, T., Ishikawa, Y., Mori, N., Nakakita, E., Yamada, T. J., Murata, A., Nakaegawa, T., and Takayabu, I.: Identifying Robust Changes of Extreme Precipitation in Japan From Large Ensemble 5-km-Grid Regional Experiments for 4K Warming Scenario, Journal of Geophysical Research: Atmospheres, 128, e2023JD038 513, https://doi.org/10.1029/2023JD038513, 2023.

https://doi.org/10.5194/egusphere-2025-6030
Preprint. Discussion started: 20 January 2026

Kim, S., Nakakita, E., Tachikawa, Y., and Takara, K.: Precipitation changes in Japan under the A1B climate change scenario, Annual Journal of Hydraulic Engineering, 54, 127–132, https://hywr.kuciv.kyoto-u.ac.jp/publications/papers/2010AJHE_Kim.pdf, 2010.

Kitamura, A., Kurikami, H., Sakuma, K., Malins, A., Okumura, M., Machida, M., Mori, K., Tada, K., Tawara, Y., Kobayashi, T., Yoshida, T., and Tosaka, H.: Redistribution and export of contaminated sediment within eastern Fukushima Prefecture due to typhoon flooding: redistribution and export of contaminated sediment, Earth Surface Processes and Landforms, 41, 1708–1726, https://doi.org/10.1002/esp.3944, 2016.

Konoplev, A., Golosov, V., Wakiyama, Y., Takase, T., Yoschenko, V., Yoshihara, T., Parenyuk, O., Cresswell, A., Ivanov, M., Carradine, M., Nanba, K., and Onda, Y.: Natural attenuation of Fukushima-derived radiocesium in soils due to its vertical and lateral migration, Journal of Environmental Radioactivity, 186, 23–33, https://doi.org/10.1016/j.jenvrad.2017.06.019, 2018.

Konoplev, A. V., Golosov, V. N., Yoschenko, V. I., Nanba, K., Onda, Y., Takase, T., and Wakiyama, Y.: Vertical distribution of radiocesium in soils of the area affected by the Fukushima Dai-ichi nuclear power plant accident, Eurasian Soil Science, 49, 570–580, https://doi.org/10.1134/S1064229316050082, 2016.

Laceby, J. P., Chartin, C., Evrard, O., Onda, Y., Garcia-Sanchez, L., and Cerdan, O.: Rainfall erosivity in catchments contaminated with fallout from the Fukushima Daiichi nuclear power plant accident, Hydrology and Earth System Sciences, 20, 2467–2482, https://doi.org/10.5194/hess-20-2467-2016, 2016a.

Laceby, J. P., Huon, S., Onda, Y., Vaury, V., and Evrard, O.: Do forests represent a long-term source of contaminated particulate matter in the Fukushima Prefecture?, Journal of Environmental Management, 183, 742–753, https://doi.org/10.1016/j.jenvman.2016.09.020, 2016b.

Lepage, H., Evrard, O., Onda, Y., Lefèvre, I., Laceby, J. P., and Ayrault, S.: Depth distribution of cesium-137 in paddy fields across the Fukushima pollution plume in 2013, Journal of Environmental Radioactivity, 147, 157–164, https://doi.org/10.1016/j.jenvrad.2015.05.003, 2015.

Loa, E. and Kawagoe, S.: Prediction of sediment production in the Abukuma River basin due to rainfall sensitivity, Tohoku journal of natural disaster science, 57, 41–45, http://nds-tohoku.in.arena.ne.jp/ndsjournal/volume57/57-8.pdf, jST Material Number F0536B, 2021.

Meusburger, K., Steel, A., Panagos, P., Montanarella, L., and Alewell, C.: Spatial and temporal variability of rainfall erosivity factor for Switzerland, Hydrology and Earth System Sciences, 16, 167–177, https://doi.org/10.5194/hess-16-167-2012, 2012.

Morino, Y., Ohara, T., Watanabe, M., Hayashi, S., and Nishizawa, M.: Episode Analysis of Deposition of Radiocesium from the Fukushima Daiichi Nuclear Power Plant Accident, Environmental Science & Technology, 47, 2314–2322, https://doi.org/10.1021/es304620x, 2013.

Nakao, A., Ogasawara, S., Sano, O., Ito, T., and Yanai, J.: Radiocesium sorption in relation to clay mineralogy of paddy soils in Fukushima, Japan, Science of The Total Environment, 468-469, 523–529, https://doi.org/10.1016/j.scitotenv.2013.08.062, 2014.

Nakao, A., Takeda, A., Ogasawara, S., Yanai, J., Sano, O., and Ito, T.: Relationships between Paddy Soil Radiocesium Interception Potentials and Physicochemical Properties in Fukushima, Japan, Journal of Environmental Quality, 44, 780–788, https://doi.org/10.2134/jeq2014.10.0423, 2015.

Nishii: The 2022 Heavy Rainfall Disaster Caused by Stagnated Linear Rainbands in the Kaetsu Region, Niigata.

Oda, T., Hotta, N., Miura, S., Endo, I., Tanoi, K., Renschler, C. S., and Ohte, N.: Redistribution of the soil ^{137} Cs inventory through litter and sediment transport on a hillslope covered by deciduous forest in Fukushima, Japan, Earth Surface Processes and Landforms, 47, 2531–2543, https://doi.org/10.1002/esp.5393, 2022.

Onda, Y., Taniguchi, K., Yoshimura, K., Kato, H., Takahashi, J., Wakiyama, Y., Coppin, F., and Smith, H.: Radionuclides from the Fukushima Daiichi Nuclear Power Plant in terrestrial systems, Nature Reviews Earth & Environment, 1, 644–660, https://doi.org/10.1038/s43017-020-0099-x, 2020.

https://doi.org/10.5194/egusphere-2025-6030
Preprint. Discussion started: 20 January 2026

Osawa, K., Nonaka, Y., Nishimura, T., Tanoi, K., Matsui, H., Mizogichi, M., and Tatsuno, T.: Quantification of dissolved and particulate radiocesium fluxes in two rivers draining the main radioactive pollution plume in Fukushima, Japan (2013–2016), Anthropocene, 22, 40–50, https://doi.org/10.1016/j.ancene.2018.04.003, 2018.

Page, T., Beven, K. J., Hankin, B., and Chappell, N. A.: Interpolation of rainfall observations during extreme rainfall events in complex mountainous terrain, Hydrological Processes, 36, e14 758, https://doi.org/10.1002/hyp.14758, 2022.

Palarz, A., James, P., Junghänel, T., Ostermöller, J., Walawender, E., and Deutschländer, T.: Radar-based heavy precipitation events in Germany and associated circulation patterns, International Journal of Climatology, 44, 196–216, https://doi.org/10.1002/joc.8323, 2024.

Panagos, P., Ballabio, C., Borrelli, P., Meusburger, K., Klik, A., Rousseva, S., Tadić, M. P., Michaelides, S., Hrabalíková, M., Olsen, P., Aalto, J., Lakatos, M., Rymszewicz, A., Dumitrescu, A., Beguería, S., and Alewell, C.: Rainfall erosivity in Europe, Science of The Total Environment, 511, 801–814, https://doi.org/10.1016/j.scitotenv.2015.01.008, 2015.

Posit team: RStudio: Integrated Development Environment for R, http://www.posit.co/, 2025.

R Core Team: A Language and Environment for Statistical Computing, https://www.R-project.org/, 2025.

Renard, K. G. and Freimund, J. R.: Using monthly precipitation data to estimate the R-factor in the revised USLE, Journal of Hydrology, 157, 287–306, https://doi.org/10.1016/0022-1694(94)90110-4, 1994.

Renard, K. G., Foster, G. R., Weesies, G. A., Mc Cool, D. K., and Yoder, D. C.: Predicting Soil Erosion by Water: A Guide to Conservation Planning with the Revised Universal Soil Loss Equation (RUSLE), no. 703 in Agriculture handbook, U.S. Department of Agriculture, Agricultural Research Service, Washington, DC, us gov. print. office edn., ISBN 0-16-048938-5 978-0-16-048938-9, https://books.google.fr/books?id=m9IIscBRmn8C&ots=QLt_XwCd5S&dq=Renard%2C%20K.G.%2C%20G.R.%20Foster%2C%20G.A.%20Weesies%2C%20D.K.%20Mc%20Cool%2C%20and%20D.C.%20Yoder.%201997.%20Predicting%20rainfall%20erosion%20by%20water%3A%20A%20guide%20to%20conservation%20planning%20with%20the%20Revised%20Universal%20Soil%20Loss%20Equation%20(RUSLE).%20Agric.%20Handb.%20703.%20US%20Gov.%20Print.%20Office%2C%20Washington%2C%20DC&lr&pg=PR5#v=onepage&q&f=false, iSSN 0065-4612, 1997.

Saito, T., Makino, H., and Tanaka, S.: Geochemical and grain-size distribution of radioactive and stable cesium in Fukushima soils: implications for their long-term behavior, Journal of Environmental Radioactivity, 138, 11–18, https://doi.org/10.1016/j.jenvrad.2014.07.025, 2014.

Sakaguchi, A., Tanaka, K., Iwatani, H., Chiga, H., Fan, Q., Onda, Y., and Takahashi, Y.: Size distribution studies of 137Cs in river water in the Abukuma Riverine system following the Fukushima Dai-ichi Nuclear Power Plant accident, Journal of Environmental Radioactivity, 139, 379–389, https://doi.org/10.1016/j.jenvrad.2014.05.011, 2015.

Shiono, T., Ogawa, S., Miyamoto, T., and Kameyama, K.: Expected impacts of climate change on rainfall erosivity of farmlands in Japan, Ecological Engineering, 61, 678–689, https://doi.org/10.1016/j.ecoleng.2013.03.002, 2013.

Suzuki, S.-i., Morooka, H., Yamazaki, T., and Iwasaki, T.: Future Projection of Extremely Heavy Rainfall in the Tohoku District of Japan with Large Ensemble Simulations Using the 5 km Regional Climate Model, Journal of Disaster Research, 19, 991–1005, https://doi.org/10.20965/jdr.2024.p0991, 2024.

Tamaoki, M., Yabe, T., Furukawa, J., Watanabe, M., Ikeda, K., Yasutani, I., and Nishizawa, T.: Comparison of Potentials of Higher Plants for Phytoremediation of Radioactive Cesium from Contaminated Soil, Environment Control in Biology, 54, 65–69, https://doi.org/10.2525/ecb.54.65, 2016.

https://doi.org/10.5194/egusphere-2025-6030
Preprint. Discussion started: 20 January 2026

Taniguchi, K., Onda, Y., Smith, H. G., Blake, W., Yoshimura, K., Yamashiki, Y., Kuramoto, T., and Saito, K.: Transport and Redistribution of Radiocesium in Fukushima Fallout through Rivers, Environmental Science & Technology, 53, 12 339–12 347, https://doi.org/10.1021/acs.est.9b02890, 2019.

Turini, N., Thies, B., Rollenbeck, R., Fries, A., Pucha-Cofrep, F., Orellana-Alvear, J., Horna, N., and Bendix, J.: Assessment of Satellite-Based Rainfall Products Using a X-Band Rain Radar Network in the Complex Terrain of the Ecuadorian Andes, Atmosphere, 12, 1678, https://doi.org/10.3390/atmos12121678, 2021.

Uchiyama, Y., Tokunaga, N., Aduma, K., Kamidaira, Y., Tsumune, D., Iwasaki, T., Yamada, M., Tadeda, Y., Ishimaru, T., Ito, Y., Watanabe, Y. W., Ikehara, K., Fukuda, M., and Onda, Y.: A storm-induced flood and associated nearshore dispersal of the river-derived suspended 137Cs, Science of The Total Environment, 816, 151 573, https://doi.org/10.1016/j.scitotenv.2021.151573, 2022.

Ueda, S., Hasegawa, H., Ohtsuka, Y., Ochiai, S., and Tani, T.: Ten-year radiocesium fluvial discharge patterns from watersheds contaminated by the Fukushima nuclear power plant accident, Journal of Environmental Radioactivity, 240, 106 759, https://doi.org/10.1016/j.jenvrad.2021.106759, 2021.

USDA–ARS: Science documentation: Revised Universal Soil Loss Equation Version 2, Science documentation, USDA–ARS, Washington, DC, 2013.

Vandromme, R., Hayashi, S., Tsuji, H., Evrard, O., Grangeon, T., Landemaine, V., Laceby, J. P., Wakiyama, Y., and Cerdan, O.: Lessons learnt on the impact of an unprecedented soil decontamination program in Fukushima on contaminant fluxes, Proceedings of the National Academy of Sciences, 120, e2301811 120, https://doi.org/10.1073/pnas.2301811120, 2023.

Wakiyama, Y., Onda, Y., Yoshimura, K., Igarashi, Y., and Kato, H.: Land use types control solid wash-off rate and entrainment coefficient of Fukushima-derived 137Cs, and their time dependence, Journal of Environmental Radioactivity, 210, 105 990, https://doi.org/10.1016/j.jenvrad.2019.105990, 2019.

Wischmeier, W. and Smith, D.: Rainfall energy and its relationship to soil loss, Eos, Transactions American Geophysical Union, 39, 285–291, https://doi.org/10.1029/TR039i002p00285, 1958.

Wischmeier, W. and Smith, D.: Predicting rainfall erosion losses. A guide to conservation planning., no. 537 in Agriculture Handbook, USDA-SEA, US. Govt. Printing Office, Washington, DC, 1978.

Yamaguchi, M., Kitamura, A., Oda, Y., and Onishi, Y.: Predicting the long-term 137Cs distribution in Fukushima after the Fukushima Dai-ichi nuclear power plant accident: a parameter sensitivity analysis, Journal of Environmental Radioactivity, 135, 135–146, https://doi.org/10.1016/j.jenvrad.2014.04.011, 2014.

Yamashiki, Y., Onda, Y., Smith, H. G., Blake, W. H., Wakahara, T., Igarashi, Y., Matsuura, Y., and Yoshimura, K.: Initial flux of sediment-associated radiocesium to the ocean from the largest river impacted by Fukushima Daiichi Nuclear Power Plant, Scientific Reports, 4, 3714, https://doi.org/10.1038/srep03714, 2014.

Yamashita, J., Enomoto, T., Yamada, M., Ono, T., Hanafusa, T., Nagamatsu, T., Sonoda, S., and Yamamoto, Y.: Estimation of soil-to-plant transfer factors of radiocesium in 99 wild plant species grown in arable lands 1 year after the Fukushima 1 Nuclear Power Plant accident, Journal of Plant Research, 127, 11–22, https://doi.org/10.1007/s10265-013-0605-z, 2014.

Yin, S., Nearing, M. A., Borrelli, P., and Xue, X.: Rainfall Erosivity: An Overview of Methodologies and Applications, Vadose Zone Journal, 16, 1–16, https://doi.org/10.2136/vzj2017.06.0131, 2017.

Yoshimura, K., Onda, Y., and Kato, H.: Evaluation of radiocaesium wash-off by soil erosion from various land uses using USLE plots, Journal of Environmental Radioactivity, 139, 362–369, https://doi.org/10.1016/j.jenvrad.2014.07.019, 2015.